

学位論文

FTO Demethylates *Cyclin D1* mRNA and Controls Cell-Cycle Progression
(FTO によるサイクリン D1 mRNA の N6 メチルアデノシン修飾を介した細胞周期の制御)

平山 真弓

Mayumi Hirayama

指導教員

中山 秀樹教授

熊本大学大学院医学教育部博士課程医学専攻歯科口腔外科学

富澤 一仁教授

熊本大学大学院医学教育部博士課程医学専攻分子生理学

2020年度

学 位 論 文

論文題名 : FTO Demethylates *Cyclin D1* mRNA and Controls Cell-Cycle Progression
(FTOによるサイクリン D1 mRNA の N6 メチルアデノシン修飾を介した細胞周期の制御)

著 者 名 : 平山 真弓
Mayumi Hirayama

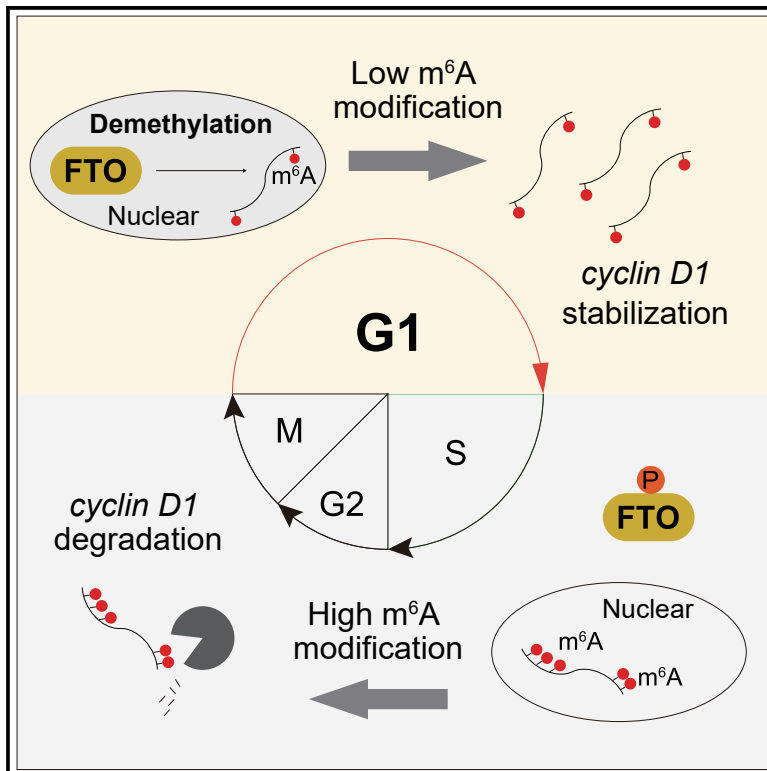
指導教員名 : 熊本大学大学院医学教育部博士課程医学専攻歯科口腔外科学 中山 秀樹教授
熊本大学大学院医学教育部博士課程医学専攻分子生理学 富澤 一仁教授

審査委員名 : 細胞医学担当教授 中尾 光善
分子遺伝学担当教授 尾池 雄一
脳神経外科学担当教授 武笠 晃文
がん代謝学担当教授 馬場 理也

2020年度

FTO Demethylates *Cyclin D1* mRNA and Controls Cell-Cycle Progression

Graphical Abstract



Authors

Mayumi Hirayama, Fan-Yan Wei, Takeshi Chujo, ..., Ryoji Yoshida, Hideki Nakayama, Kazuhito Tomizawa

Correspondence

fywei@kumamoto-u.ac.jp, fanyan.wei.d3@tohoku.ac.jp (F.-Y.W.), tomikt@kumamoto-u.ac.jp (K.T.)

In Brief

Hirayama et al. show that FTO, the demethylase for m⁶A modification, regulates G1 cell-cycle progression by targeting *cyclin D1* mRNA. Their studies indicate that m⁶A modification of mRNA can be periodically regulated during the cell cycle and that m⁶A demethylase FTO may be a therapeutic target for cancer treatment.

Highlights

- FTO deficiency suppresses *cyclin D1* mRNA levels and induces a prolonged G1 phase
- FTO demethylates m⁶A-modified *cyclin D1* mRNA and sustains its expression
- m⁶A modification of *cyclin D1* mRNA oscillates in a cell-cycle-dependent manner
- Nucleocytoplasmic shuttling of FTO regulates *cyclin D1* m⁶A modification



FTO Demethylates *Cyclin D1* mRNA and Controls Cell-Cycle Progression

Mayumi Hirayama,^{1,2} Fan-Yan Wei,^{1,3,7,9,*} Takeshi Chujo,¹ Shinya Oki,^{3,4,8} Maya Yakita,^{1,2} Daiki Kobayashi,⁵ Norie Araki,⁵ Nozomu Takahashi,² Ryoji Yoshida,² Hideki Nakayama,² and Kazuhito Tomizawa^{1,6,*}

¹Department of Molecular Physiology, Faculty of Life Sciences, Kumamoto University, Kumamoto-Shi, Kumamoto 860-8556, Japan

²Department of Oral and Maxillofacial Surgery, Faculty of Life Sciences, Kumamoto University, Kumamoto-Shi, Kumamoto 860-8556, Japan

³Precursory Research for Embryonic Science and Technology (PRESTO), Japan Science and Technology Agency (JST), Kawaguchi-Shi, Saitama 332-0012, Japan

⁴Department of Developmental Biology, Graduate School of Medical Sciences, Kyushu University, Fukuoka-Shi, Fukuoka 812-8582, Japan

⁵Department of Tumor Genetics and Biology, Faculty of Life Sciences, Kumamoto University, Kumamoto-Shi, Kumamoto 860-8556, Japan

⁶Center for Metabolic Regulation of Healthy Aging, Faculty of Life Sciences, Kumamoto University, Kumamoto-Shi, Kumamoto 860-8556, Japan

⁷Department of Modomics Biology and Medicine, Institute of Development, Aging and Cancer, Tohoku University, Sendai-Shi, Miyagi 980-8575, Japan

⁸Present address: Department of Drug Discovery Medicine, Kyoto University Graduate School of Medicine, Kyoto 606-8507, Japan

⁹Lead Contact

*Correspondence: fywei@kumamoto-u.ac.jp or fanyan.wei.d3@tohoku.ac.jp (F.-Y.W.), tomikt@kumamoto-u.ac.jp (K.T.)

<https://doi.org/10.1016/j.celrep.2020.03.028>

SUMMARY

N⁶-Methyladenosine (m⁶A) modification is the major chemical modification in mRNA that controls fundamental biological processes, including cell proliferation. Herein, we demonstrate that fat mass and obesity-associated (FTO) demethylates m⁶A modification of cyclin D1, the key regulator for G1 phase progression and controls cell proliferation in vitro and in vivo. FTO depletion upregulates cyclin D1 m⁶A modification, which in turn accelerates the degradation of cyclin D1 mRNA, leading to the impairment of G1 progression. m⁶A modification of cyclin D1 oscillates in a cell-cycle-dependent manner; m⁶A levels are suppressed during the G1 phase and enhanced during other phases. Low m⁶A levels during G1 are associated with the nuclear translocation of FTO from the cytosol. Furthermore, nucleocytoplasmic shuttling of FTO is regulated by casein kinase II-mediated phosphorylation of FTO. Our results highlight the role of m⁶A in regulating cyclin D1 mRNA stability and add another layer of complexity to cell-cycle regulation.

INTRODUCTION

N⁶-Methyladenosine (m⁶A) is the most abundant chemical modification present in mammalian mRNA and is involved in various steps of gene expression regulation (Fu et al., 2014; Meyer and Jaffrey, 2014; Zhao et al., 2017). The m⁶A modification is added by m⁶A methyltransferase “writers” that interact with specific adaptor protein “readers” and removed by demethylase “erasers”. Methyltransferases form a multicomponent complex consisting of methyltransferase-like 3 (METTL3) and METTL14 that interacts with accessory proteins including Wilms tumor 1-associating pro-

tein (WTAP) and RNA-binding protein 15 (RBM15), and catalyze m⁶A modification of mRNA possessing the consensus RRACH motif (R = G or A; H = A, C, or U) (Dominissini et al., 2012; Liu et al., 2014; Ping et al., 2014). In addition to METTL3/14, METTL16 has recently been identified as a m⁶A writer that can modify structured RNA (Mendel et al., 2018). Once methylated, various reader proteins such as the YTH domain family proteins YTHDF1–3 directly bind to m⁶A modifications (Li et al., 2017a; Zhu et al., 2014) and initiate diverse biological processes, including pre-mRNA splicing, mRNA degradation, and translational control (Wang et al., 2014; Xiao et al., 2016). The m⁶A modification is widespread in various mRNA regions, including the 5' untranslated region (5' UTR), exons, and the 3' UTR (Dominissini et al., 2012). m⁶A has been linked to mRNA degradation; in *Mettl3* knockout (KO) embryonic stem cells, deletion of m⁶A results in a 4- to 8-fold increase in the half-life of mRNA (Ke et al., 2017). Degradation of m⁶A-containing mRNA is in part mediated by the binding of YTHDF2 to the m⁶A site. In *YTHDF2* knockdown cells, the half-life of m⁶A-containing mRNA is increased by ~30% (Wang et al., 2014). Similarly, the reader protein YTHDC2 selectively binds to m⁶A sites in its target mRNA, leading to its degradation (Hsu et al., 2017; Wojtas et al., 2017).

Fat mass and obesity-associated (FTO) and alkB homolog 5 (ALKBH5) are the erasers for m⁶A modifications (Fu et al., 2013; Jia et al., 2011; Zheng et al., 2013). Although these two erasers are expressed ubiquitously, their physiological functions appear to differ. Constitutive *Alkbh5* KO mice are viable and anatomically normal, but they display hypofertility due to the elevation of m⁶A in genes related to spermatogenesis, resulting in aberrant splicing and rapid degradation of the corresponding mRNAs and leading to the depletion of germ cells (Zheng et al., 2013; Tang et al., 2018). By contrast, *FTO* KO mice are viable and fertile, but exhibit a reduction in adipose tissue volume and lean body mass (Fischer et al., 2009; Zhao et al., 2014; Merkestein et al., 2015), likely due to a decrease in the proliferation of adipocytes (Wu et al., 2018). In humans, the effects of *FTO* deficiency are more profound than in the mouse model; loss of *FTO* function



in human embryos is associated with a severe growth defect that results in premature death (Fischer et al., 2009; Boissel et al., 2009). By contrast, a gain of *FTO* function has been associated with aberrant cell proliferation in many types of tumors, including gastric cancer and acute myeloid leukemia (Li et al., 2017b; Xu et al., 2017). These results strongly suggest that erasure of m⁶A by *FTO* is required for effective cell proliferation control.

Cell proliferation is the consequence of cell-cycle progression. The cell cycle is tightly controlled by cell-cycle-specific cyclins and their cyclin-dependent kinase (CDK)-binding partners (Bertoli et al., 2013). The progression of the G1 phase is mainly controlled by cyclin D1 and Cdk4/6, which phosphorylate retinoblastoma protein (RBP), leading to the release of E2F transcription factors (Hydbring et al., 2016). Cdk2/cyclin E controls progression from the G1 phase to the S phase, Cdk2/cyclin A controls progression from the S phase to the G2 phase, and Cdk1/cyclin A/B controls progression from the G2 and M phases. While CDKs are stable throughout the cell cycle, each cyclin is temporospatially controlled at the protein level. For example, cyclin D1 is localized in the nucleus and reaches its maximum level before the S phase (Baldin et al., 1993). At the end of the G1 phase and after entry of the S phase, cyclin D1 protein is exported to the cytoplasm and degraded by the ubiquitin-proteasome system (Lin et al., 2006; Fasanaro et al., 2010).

Similar to the oscillation of cyclin proteins, mRNAs of cyclins also oscillate during the cell cycle (Liu et al., 2017). These periodic changes in mRNAs are in part controlled at the transcriptional level and are coupled to CDK activities (Lim and Kaldis, 2013). During the G1 phase, Cdk4/cyclin D1-mediated phosphorylation of the RBP activates E2F, leading to the transcription of cyclin A/E, which is required for G1/S transition. During the G2 phase, Cdk2/cyclin A phosphorylates FoxM1, which drives the transcription of cyclin B. However, although the transcription network that drives the periodic expression of cell-cycle-related mRNAs is well understood, little is known about the regulatory mechanism of these mRNAs at the post-transcriptional level, which is emerging as a novel regulatory mechanism of gene expression that potentially influences cell-cycle progression.

Given the implications of *FTO* regulating the methylation status of mRNA as well as cell proliferation, here, we investigated whether the cell cycle is controlled by *FTO* at the post-transcriptional level and explored the potential molecular mechanism by identifying mRNA targets and m⁶A sites. The findings demonstrate that *FTO* regulates G1 phase progression by modulating m⁶A modification of *cyclin D1*.

RESULTS

Silencing of *FTO* Impairs the Cell Cycle

To investigate the impact of *FTO* deficiency on cell proliferation and the cell cycle, we knocked down *FTO* using small interfering RNAs (siRNA). *FTO* knockdown significantly suppressed the cell growth of HOC313 cells (cell growth at day 6: si*FTO*#1: 2.9 ± 0.07 , si*FTO*#2: 2.5 ± 0.07 versus siControl: 4.3 ± 0.19 ; Figure 1A), MDA-MB-231 cells (cell growth at day 5: si*FTO*: 1.4 ± 0.03 versus siControl: 2.0 ± 0.05 ; Figure S1A), and SAS cells (cell growth at day 5: si*FTO*: 1.1 ± 0.03 versus siControl: 3.5 ± 0.15 ; Figure S1B). We confirmed that *FTO*-siRNAs successfully dysregulated m⁶A

modification of mRNAs isolated from *FTO* knockdown cells by dot blot analysis (si*FTO*: 1.3 ± 0.07 change versus siControl: 1.0 ± 0.04) and liquid chromatography-tandem mass spectrometry (LC-MS/MS; si*FTO*: 1.2 ± 0.03 change versus siControl: 1.0 ± 0.03 ; Figures S1C–S1E), suggesting that the suppression of cell growth was due to the loss of *FTO* function. To examine the impact of *FTO* knockdown on the cell cycle, we performed flow cytometry analysis and observed an increase in the number of cells in the G1 phase, coupled with a decrease in the number of cells in the non-G1 phase (G2/M/S), upon *FTO* knockdown compared with control cells (Figure 1B). Next, we induced fluorescent ubiquitination-based cell-cycle indicators (FUCCI) to track the individual phase (Figure 1C) (Sakaue-Sawano et al., 2008). These indicators can illuminate cells in G1 using monomeric Kusabira-Orange (mKO) and in other phases (S/G2/M) using monomeric Azami-Green (mAG; Figure 1C). In the control cells, mKO and mAG alternated, reflecting normal cell-cycle progression. However, in *FTO* knockdown cells, mKO fluorescence was prolonged and mAG fluorescence was diminished (Figures 1D–1G). These results suggest that *FTO* knockdown slows cell proliferation by impairing G1 phase progression.

FTO Knockdown Suppresses Cell-Cycle-Related Genes and Alters the m⁶A Profile of *Cyclin D1*

Next, we performed a comprehensive RNA sequencing (RNA-seq) analysis to investigate transcriptome changes in control and *FTO* knockdown cells. We selected the most influential genes based on absolute fold-change >2 and adjusted $p < 0.05$. Consequently, 349 genes were significantly downregulated and 255 genes were significantly upregulated in *FTO* knockdown cells compared with control cells (Figures 2A and S2A). Kyoto Encyclopedia of Genes and Genomes (KEGG) pathway analysis showed that downregulated genes were significantly correlated with the cell cycle and tumorigenesis (Figure 2B). Meanwhile, upregulated genes were correlated with metabolic pathways, although the enrichment score was relatively low (Figure S2B).

Next, we performed m⁶A-specific methylated RNA immunoprecipitation sequencing (MeRIP-seq) to examine whether these differentially regulated genes were associated with m⁶A modifications in mRNA, among which 195 genes overlapped with those upregulated upon *FTO* knockdown (Figure S2B). These genes were correlated with metabolic regulation, but they were few in number and the enrichment score was again low (Figure S2C). Meanwhile, 227 genes overlapped with those downregulated upon *FTO* knockdown (Figure 2C), and pathway analysis revealed that many were related to the cell cycle (Figure 2D), of which *cyclin D1* showed the highest level of m⁶A modification (Figure 2E). *Cyclin D1* contains m⁶A sites in both the 5' UTR and 3' UTR, with the level significantly higher in the 5' UTR (Figure 2F). The presence of m⁶A modifications in *cyclin D1* was further confirmed in MeRIP-seq analyses of HepG2 cells, HEK293 cells, and HeLa cells, conducted by independent groups, with the results deposited in the MeT-DB public database (Figure S2D). Similar to our result, these results also showed an enrichment of m⁶A in the 5' UTR compared with the 3' UTR (Figure S2D). To confirm whether m⁶A modification of *cyclin D1* is regulated by *FTO*, MeRIP-seq was performed to compare the m⁶A density of *cyclin D1* in cells with or without

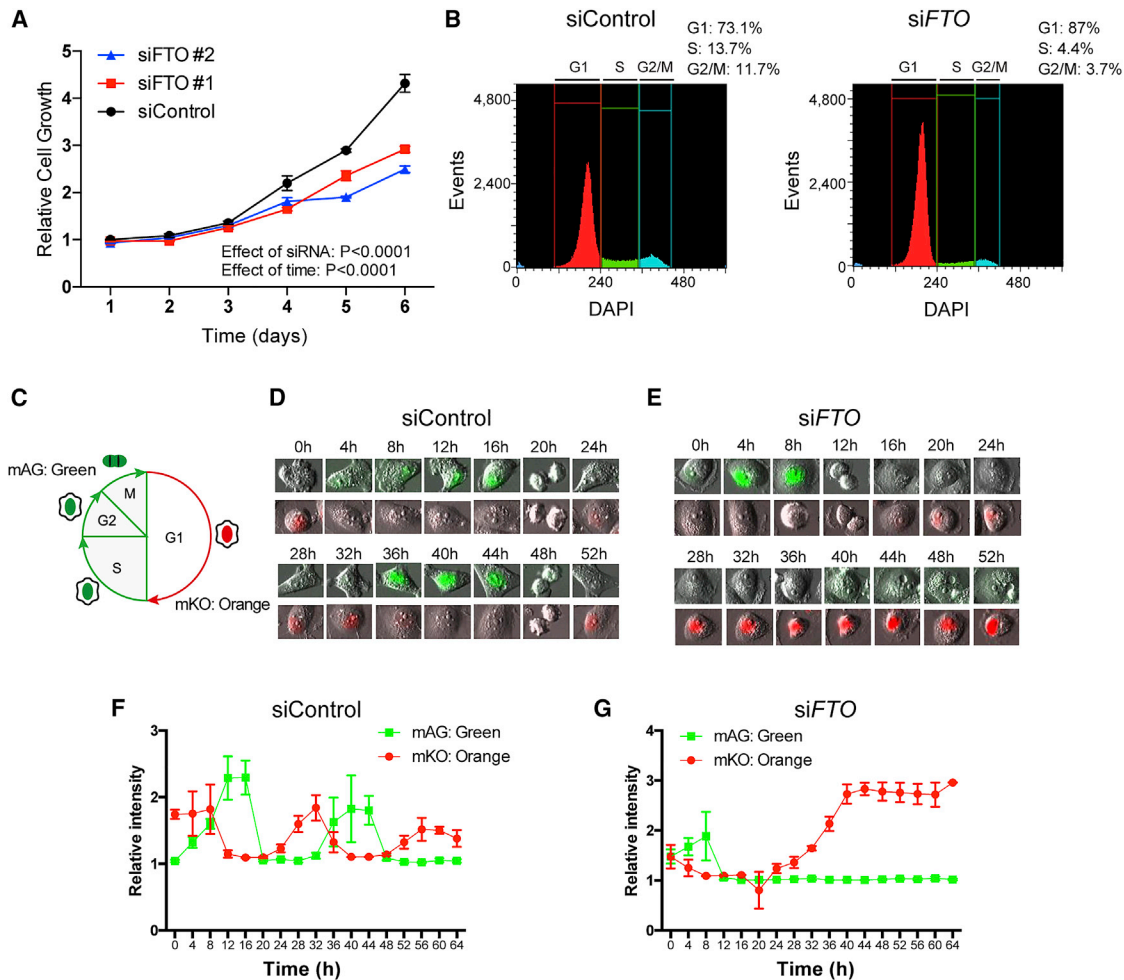


Figure 1. Silencing of *FTO* Impairs Cell-Cycle Progression

(A) Relative cell growth of HOC313 cells transfected with control siRNA (siControl) or siRNAs targeting *FTO* (siFTO, n = 4 for each group). (B) HOC313 cells were treated with siControl or siFTO#1 for 4 days, and the cell cycle was examined by flow cytometry. Representative images are shown. (C) Illustration of FUCCI-expressing HOC313 cells at each cell-cycle phase. Cells at G1 display orange fluorescence from mKO, while cells at non-G1 phases (S, G2, and M) display green fluorescence from mAG. (D and E) Cell-cycle-dependent changes in fluorescence in HOC313 cells transfected with siControl (D) or siFTO#1 (E). Prolonged existence of mKO fluorescence was observed in *FTO* knockdown HOC313 cells. (F and G) Quantitation of mAG and mKO fluorescence in HOC313 cells transfected with siControl (F) or siFTO #1 (G). n = 3 from 3 biological replicates. Data are represented as means \pm SEMs.

FTO knockdown. The m⁶A density of *cyclin D1* in *FTO* knockdown cells was higher than that in control cells (Figure 2G). To validate and quantitate this result, total RNA was isolated from control and *FTO* knockdown cells and subjected to MeRIP-qPCR. Similar to the MeRIP-seq results, m⁶A levels in both the 5' UTR and 3' UTR were significantly enhanced upon *FTO* knockdown, suggesting that *FTO* is responsible for the demethylation of m⁶A in *cyclin D1* (5' UTR: siFTO 4.7 \pm 1.3 versus siControl: 1.0 \pm 0.2; 3' UTR: siFTO 5.3 \pm 0.38 versus siControl: 1.0 \pm 0.07; Figure 2H).

m⁶A Modification Promotes Degradation of *Cyclin D1*

The upregulation of m⁶A has been associated with mRNA instability and degradation and with promoting protein translation (Wang et al., 2014, 2015). To examine the impact of m⁶A modifi-

cation on the expression of *cyclin D1*, we investigated *cyclin D1* expression at both mRNA and protein levels, and both were significantly decreased in *FTO* knockdown cells (Figures 3A–3C). Suppression at both mRNA and protein levels was also confirmed in other cell lines (Figures S3A–S3C). We then examined the stability of *cyclin D1* using actinomycin D, an inhibitor of RNA transcription. A rapid decrease in *cyclin D1* was observed in *FTO* knockdown cells in the presence of actinomycin D compared with control cells (Figure 3D). The forced expression of *FTO* in *FTO* knockdown cells was sufficient to rescue *cyclin D1* levels (Figures S3D and S3E), suggesting that *FTO* is involved in regulating *cyclin D1* levels through m⁶A demethylation.

Next, we sought to modify the m⁶A sites of the *cyclin D1* gene to elucidate the causal role of m⁶A modification in the regulation

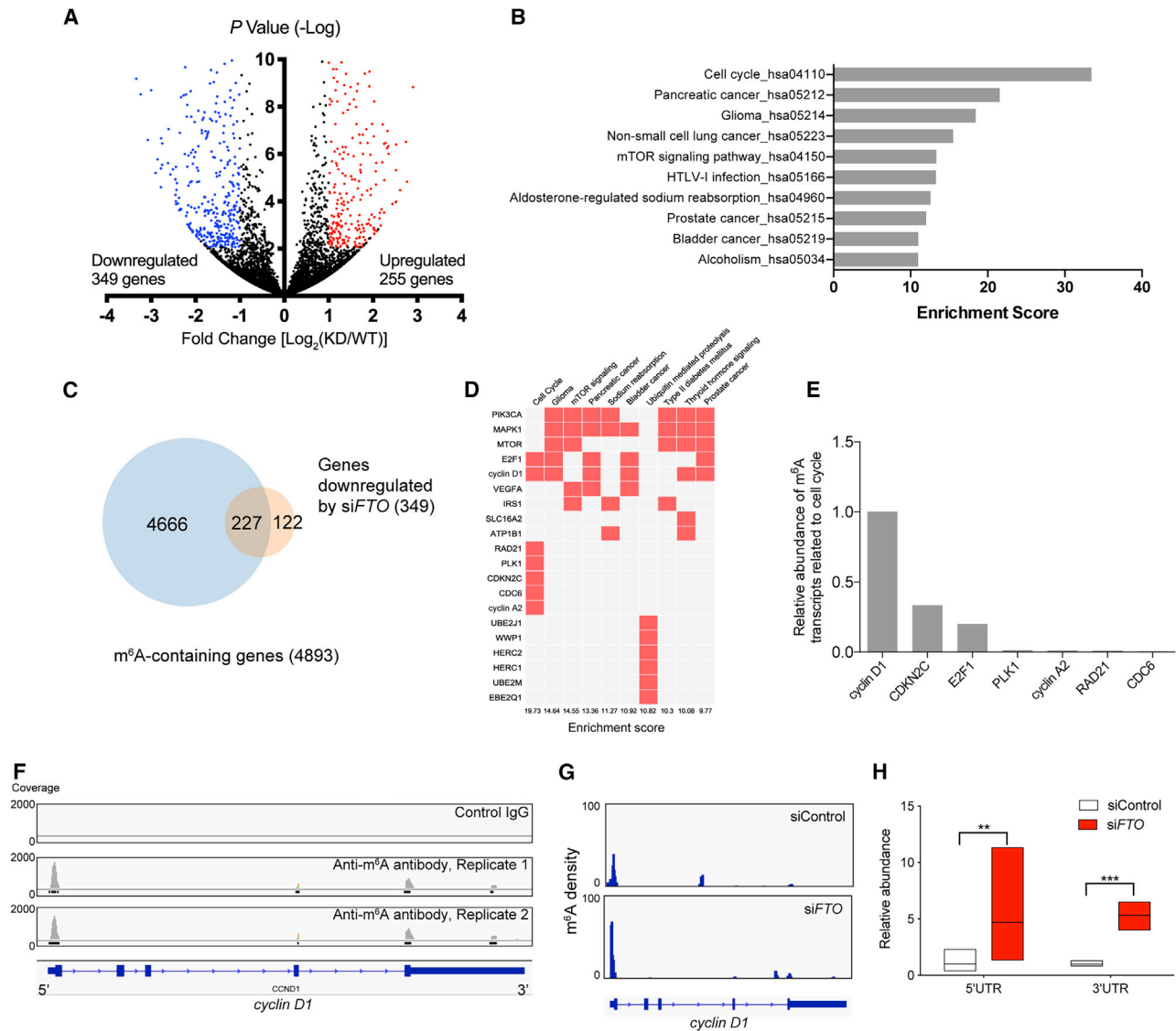


Figure 2. FTO Knockdown Suppresses Cell-Cycle-Related Genes and Alters the m⁶A Profile of Cyclin D1

(A) Volcano plot comparing gene expression in cells transfected with siControl and siFTO#1. Blue and red dots indicate significantly altered genes in FTO knockdown cells (>2-fold change, adjusted $p < 0.05$).

(B) Pathway analysis of genes downregulated in FTO knockdown cells.

(C) MeRIP-seq analysis of control cells to identify m⁶A-containing genes. The Venn diagram shows an overlap between genes containing m⁶A modifications and genes downregulated in FTO knockdown cells.

(D) Pathway analysis of the 227 m⁶A-containing genes downregulated in FTO knockdown cells. The top 20 genes enriched in pathways are shown.

(E) Comparison of the abundance of m⁶A modifications in genes related to the cell cycle.

(F) MeRIP-seq analysis using m⁶A-specific antibody or control immunoglobulin G (IgG) in control HOC313 cells. Representative m⁶A peaks of the *cyclin D1* gene are shown. Note that m⁶A peaks were detected by anti-m⁶A antibody, but not by the control IgG.

(G) MeRIP-seq analysis of HOC313 cells treated with siControl and siFTO#1. Note that the density of m⁶A in *cyclin D1* is higher in FTO knockdown cells than in control cells.

(H) Relative abundance of m⁶A in the 5' UTR and 3' UTR of *cyclin D1* examined in cells treated with siControl and siFTO#1, analyzed by MeRIP-qPCR ($n = 6-9$ for each group; ** $p < 0.01$, *** $p < 0.001$ by Student's t test).

Data are represented as means \pm SEMs.

of *cyclin D1* stability. *Cyclin D1* contains the RRACH m⁶A consensus motif in both the 5' UTR and the 3' UTR (Dominissini et al., 2012). We noticed that there is a putative m⁶A motif (GGACT) located 202 nt upstream of the start codon that is

completely conserved in mammals (Figures 4A and S4A). Given the potential importance of this motif, we applied CRISPR-Cas9 to directly edit the m⁶A sites in the *cyclin D1* gene. We obtained a biallelic edited clone with 1–2 nt deleted immediately after the

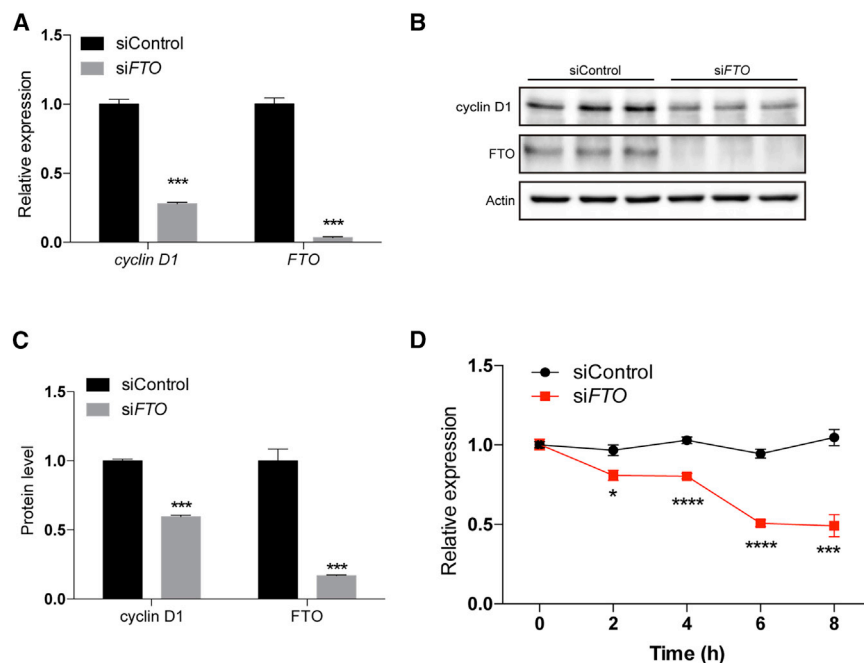


Figure 3. Regulation of Cyclin D1 mRNA Stability by m⁶A Modification

(A) Relative expression levels of *cyclin D1* and *FTO* in HOC313 cells treated with siControl and siFTO#1 (*cyclin D1*: siFTO#1: 0.28 ± 0.01 versus control: 1.0 ± 0.03; *FTO*: siFTO#1 0.035 ± 0.006 versus control: 1.0 ± 0.04, n = 3 for each group; ***p < 0.001 by Student's t test).

(B) Protein levels of cyclin D1 and FTO examined by western blotting in HOC313 cells treated with siControl and siFTO#1.

(C) Quantitation of cyclin D1 and FTO protein levels (cyclin D1: siFTO#1: 0.60 ± 0.01 versus control: 1.0 ± 0.01, *FTO*: siFTO#1 0.17 ± 0.005 versus control: 1.0 ± 0.09, n = 3 for each group; ***p < 0.001 by Student's t test).

(D) Control HOC313 cells (siControl) and *FTO* knockdown HOC313 cells (siFTO) were treated with actinomycin D for the indicated times, and the relative expression levels of *cyclin D1* are shown (siFTO: 0.81 ± 0.03 at 2 h, 0.8 ± 0.02 at 4 h, 0.51 ± 0.02 at 6 h, 0.49 ± 0.07 at 8 h versus siFTO at 0 h, siControl: 0.97 ± 0.03 at 2 h, 1.0 ± 0.02 at 4 h, 0.95 ± 0.03 at 6 h, 1.0 ± 0.05 at 8 h versus siControl at 0 h, n = 6 for each group; *p < 0.05, ***p < 0.001, ****p < 0.0001 by repeated-measure of 2-way ANOVA followed by multiple comparison tests).

m⁶A sites (Figure 4B). The deletions converted the canonical GGACT motif to the non-canonical GGAGT and GGACG sequences (Figure 4B). As expected, MeRIP-qPCR results showed that m⁶A levels in the 5' UTR of mutant *cyclin D1* (*Mut-cyclin D1*) mRNA were significantly decreased compared with those in wild-type (WT) *cyclin D1* (*Mut-cyclin D1*: 0.18 ± 0.008 versus WT: 1.0 ± 0.17; Figure 4C). Moreover, knockdown of FTO did not further downregulate m⁶A levels in the 5' UTR of *Mut-cyclin D1* (Figure S4B), suggesting that gene editing resulted in a permanent suppression of m⁶A modification. The decrease in m⁶A levels increased the stability of *Mut-cyclin D1* mRNA (*Mut-cyclin D1*: 0.97 ± 0.02 at 8 h versus 0 h, WT: 0.62 ± 0.02 at 8 h versus 0 h; Figure 4D), as well as its steady-state expression level (*Mut-cyclin D1*: 1.4 ± 0.06 versus WT: 1.0 ± 0.04; Figure 4E). Accordingly, cells expressing *Mut-cyclin D1* experienced a shortened G1 phase (WT: 11.6 ± 0.1 h versus *Mut-cyclin D1*: 9.3 ± 0.4 h; Figure 4F), which led to an increase in cell proliferation compared with cells expressing WT *cyclin D1* (WT: 2.8 ± 0.20 versus *Mut-cyclin D1*: 3.8 ± 0.15 at day 5; WT: 2.5 ± 0.18 versus *Mut-cyclin D1*: 3.6 ± 0.12 at day 6; Figure 4G). These results provide direct evidence that FTO-mediated demethylation of m⁶A modification of *cyclin D1* mRNA regulates its stability and thereby affects its steady-state expression level, and hence cell-cycle progression.

Loss of FTO1 Suppresses Cell Growth In Vivo

The inhibitory effect of *FTO* knockdown on cell growth prompted us to examine whether *FTO* deficiency attenuates cell growth *in vivo*. To this end, we generated an *FTO* KO SAS cell line using CRISPR-Cas9. We chose SAS cells because HOC313 cells did not form solid tumors in nude mice (data not shown). This KO cell line contains a single nucleotide insertion in exon 3 of the *FTO* gene, which results in a reading frameshift and incorpora-

tion of a premature stop codon (Figure 5A). In accordance with the change in genomic sequence, the *FTO* protein was completely absent in *FTO* KO cells (Figure 5B). *FTO* deficiency upregulated m⁶A modification levels in the 5' UTR of *cyclin D1* (WT: 1.0 ± 0.08 versus *FTO* KO: 1.7 ± 0.28; Figure 5C), which was associated with a decrease in mRNA stability (WT: 0.91 ± 0.04 versus *FTO* KO 0.73 ± 0.01; Figure 5D) and steady-state protein level (Figure 5B). To examine cell-cycle progression, *FTO*-deficient cells were transfected with the FUCCI reporter, and the duration of the G1 phase was measured. Similar to *FTO* knockdown cells, these cells also displayed a prolonged G1 phase (WT: 7.7 ± 0.09 h versus *FTO* KO: 11 ± 0.67 h; Figure 5E). Accordingly, *FTO* KO cells exhibited a significant decrease in cell proliferation compared with WT cells (WT: 2.8 ± 0.2 versus *FTO* KO: 1.7 ± 0.06 at day 3; WT: 5.7 ± 0.16 versus *FTO* KO: 3.4 ± 0.33 at day 4; WT: 7.7 ± 0.38 versus *FTO* KO: 5.6 ± 0.16 at day 5; Figure 5E). Finally, we subcutaneously implanted WT and *FTO* KO cells in nude mice and monitored cell growth *in vivo* for 2 weeks. While WT cells successfully formed large solid tumors, *FTO* KO cells only formed small tumors, the weight of which was nearly one-tenth that of WT tumors (WT: 0.53 ± 0.06 g versus *FTO* KO: 0.066 ± 0.005 g; Figures 5G and 5H). These results suggest that *FTO* is important for cell-cycle progression *in vitro* and *in vivo*.

m⁶A Modification of Cyclin D1 Is Differentially Regulated during the Cell Cycle

Given the important role of FTO-mediated demethylation of *cyclin D1* in regulating G1 progression and in cell proliferation, we sought to investigate whether m⁶A modification of *cyclin D1* is differentially regulated in G1 and non-G1 phases in the normal cell cycle. Taking advantage of FUCCI technology, we sorted cells into mKO-expressing cells (orange in the G1 phase)

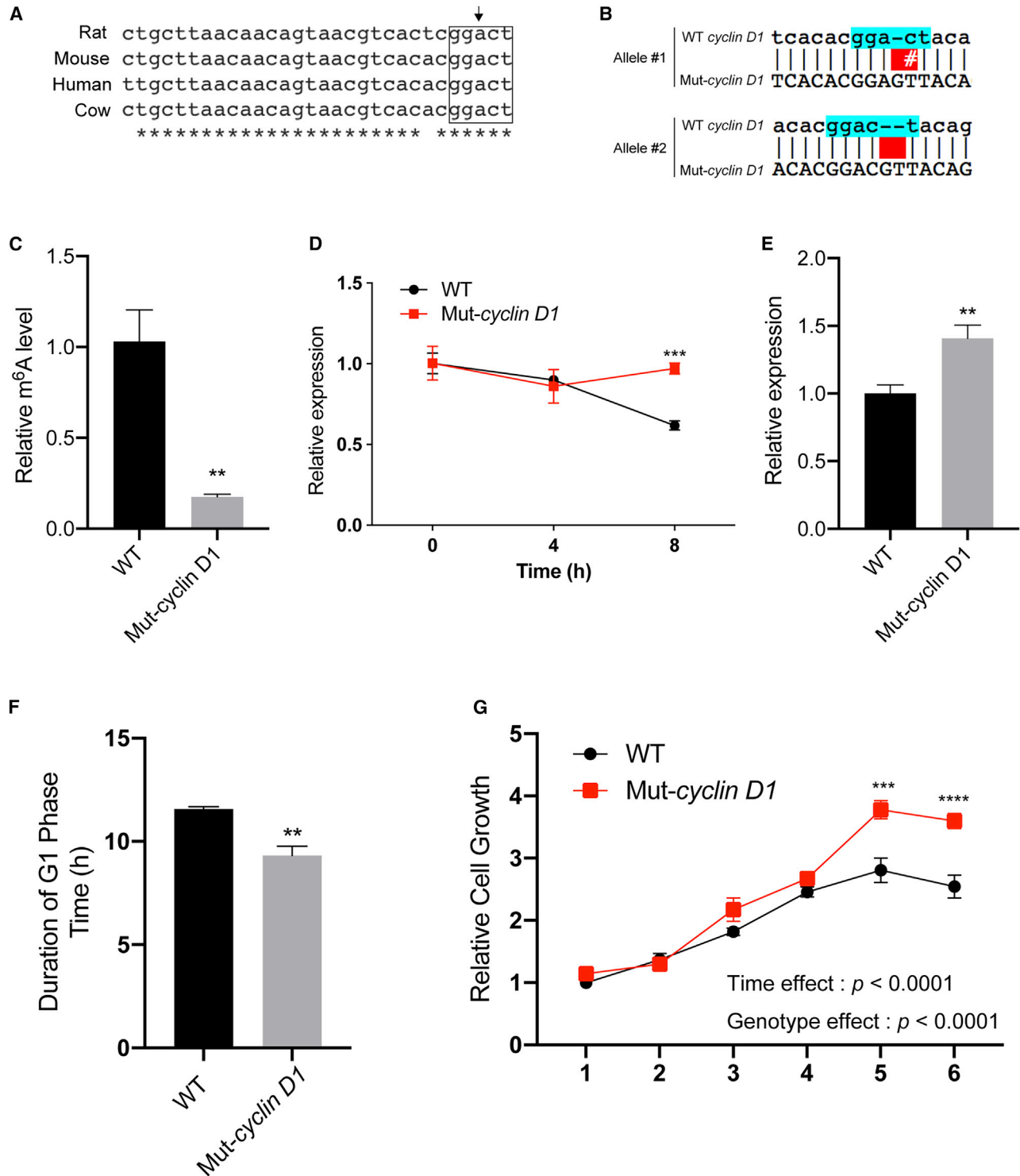


Figure 4. Genomic Editing of m⁶A Modification Sites

(A) Alignment of the 5' UTR sequences of *cyclin D1* in rat, mouse, human, and cow genomes. The conserved m⁶A consensus motif is boxed, and the arrow indicates the potential m⁶A site.

(B) Alignment of genomic sequences of wild-type (WT) and mutant *cyclin D1* (Mut-*cyclin D1*) genes edited by CRISPR-Cas9. The m⁶A motifs in the WT *cyclin D1* gene are highlighted in blue.

(C) The m⁶A level surrounding the edited site was examined by MeRIP-qPCR. Note that the m⁶A level in mutated *cyclin D1* (Mut-*cyclin D1*) is significantly lower than that in WT *cyclin D1* (n = 3 for each group; **p < 0.01 by Student's t test).

(legend continued on next page)

and mAG-expressing cells (green in the non-G1 [G2/M/S] phase) using fluorescence-activated cell sorting (FACS; Figure 6A). Expression of *cyclin D1* in the G1 phase was higher than in the non-G1 phase at both mRNA (non-G1: 1.0 ± 0.03 versus G1: 1.2 ± 0.02 ; Figure 6A) and protein levels (non-G1: 1.0 ± 0.03 versus G1: 2.8 ± 0.26 ; Figures 6B and 6C), indicating that cell sorting was successful. The m⁶A level of *cyclin D1* in G1 and non-G1 phases was then examined by MeRIP-qPCR, and the level was significantly lower in G1 (non-G1: 1.0 ± 0.16 versus G1: 0.41 ± 0.07 ; Figure 6D). Thus, the m⁶A level appears to be inversely correlated with the levels of *cyclin D1* in G1 and non-G1 phases. In addition, we synchronized the cell cycle at the G1/S phase boundary by treating cells with thymidine (Satoh and Kaida, 2016). *Cyclin D1* mRNA and protein levels gradually increased after release from cell-cycle blocking, and peaked at 20 h after release (*cyclin D1* mRNA levels: 1.0 ± 0.06 at 0 h, 1.4 ± 0.003 at 16 h, 1.4 ± 0.01 at 20 h; Figures 6E and 6F). We collected cells at 0 and 20 h after cell-cycle release for MeRIP-qPCR analysis, and m⁶A modification of *cyclin D1* at the 20 h point was significantly lower than that at 0 h (Figure 6G). Again, the m⁶A level was inversely correlated with the level of *cyclin D1* at each time point (m⁶A levels: 1.0 ± 0.07 at 0 h versus 0.7 ± 0.06 at 20 h; Figure 6G).

Differential Localization of FTO during G1 and Non-G1 Phases

Finally, we sought to elucidate the molecular mechanism underlying the cell-cycle-dependent oscillation of m⁶A in *cyclin D1*. We predicted that differences in m⁶A modification of *cyclin D1* in G1 and non-G1 phases may reflect the differential expression of FTO. However, FTO levels did not differ between G1 and non-G1 phases (Figure S5A). We performed immunostaining of FTO to investigate whether the level and subcellular localization of FTO could be differentially regulated during the cell cycle. The total fluorescence of FTO did not differ between mAG⁺ (non-G1 phase) and mKO⁺ (G1 phase) cells (Figure S5B). Nevertheless, FTO exhibited differential subcellular localization in these cells; FTO accumulated in the cytosol in mAG⁺ cells, but it accumulated in the nucleus of mKO⁺ cells (Figures 7A–7D). Quantitative analysis of the relative FTO intensity revealed preferential and significant accumulation in the nucleus during the G1 phase (non-G1: 0.51 ± 0.07 versus G1: 1.0 ± 0.07 ; Figure 7E). Furthermore, strong nuclear FTO staining was associated with strong nuclear cyclin D1 staining in the G1 phase (Figure S5C). To explore whether FTO localization affected the interaction between FTO and *cyclin D1*, the FTO-RNA complex in nuclear and cytosol fractions was immunoprecipitated, and RT-PCR was subsequently performed to detect FTO-bound *cyclin D1*.

The FTO-*cyclin D1* complex was detected in the nuclear fraction, but not in the cytosolic fraction (Figure 7F). These results suggest that nuclear FTO binds to *cyclin D1* mRNA to remove its m⁶A modification and increase its stability during the G1 phase, while cytosolic FTO is not accessible to *cyclin D1* mRNA, which in turn induces m⁶A modification of *cyclin D1*, leading to its destabilization during the non-G1 phase.

Regulation of FTO Localization by Phosphorylation

Given the dynamic nucleocytoplasmic shuttling of FTO, we sought to investigate the molecular mechanism. A previous study showed that the N terminus of FTO, corresponding to amino acids (aa) 1–31, contains a nuclear localization signal (NLS) (Aas et al., 2017). In addition, we found that an internal region of FTO (aa 141–155) contains a potential nuclear export signal (NES). We therefore hypothesized that post-translational modification, such as phosphorylation, of amino acids within or near the NLS and NES may be responsible for the nucleocytoplasmic shuttling of FTO. To explore this, we searched for potential phosphorylation sites within the NLS and NES and found that Thr 4, Thr 6, and Thr 150 are reportedly phosphorylated in cells. Notably, Thr 4 and Thr 6 are conserved in mammals, and Thr 150 is highly conserved in vertebrates (Han et al., 2010). To investigate whether phosphorylation at these sites is responsible for nucleocytoplasmic shuttling, we generated FTO mutants carrying Thr-to-Ala mutations at each site (T4A, T6A, and T150A) to mimic the dephosphorylated form. Similar to the cellular distribution of FTO WT, FTO T4A and FTO T6A were preferentially localized in the cytosol, while nuclear localization was observed occasionally (Figures 7G, 7H, and S6A). By contrast, the FTO T150A mutant was preferentially localized in the nucleus (nuclear localization of T150A: $67\% \pm 9.7\%$ versus WT: $24\% \pm 1.8\%$; Figures 7G, 7H, and S6A). We also engineered the Thr-to-Glu mutation at Thr 150 (T150E) to mimic the phosphorylated form of FTO, and in contrast to FTO T150A, FTO T150E displayed cytosolic localization (nuclear localization of T150E: $1.6\% \pm 0.66\%$; Figures 7G, 7H, and S6B). It should be noted that the fluorescence intensity of FTO T150E appeared to be lower than that of FTO T150A. The low fluorescence intensity of FTO T150E could be attributed to its diffused localization in cytosol, which may cause a decrease in the overall fluorescence intensity, as reported in a previous study (Aas et al., 2017). The expression of the FTO T150E mutant significantly increased m⁶A in *cyclin D1*, which suggests that *cyclin D1* was not accessible to the FTO T150E mutant (WT: 1.0 ± 0.08 versus T150E: 1.7 ± 0.25 ; Figure 7I). In agreement with these results, transient expression of WT FTO and nuclear localization of the FTO 150A mutant partially rescued the growth defect of FTO KO cells, while cytosol

(D) WT and mutant HOC313 cells expressing edited *cyclin D1* (Mut-*cyclin D1*) were treated with actinomycin D for the indicated times, and the relative expression levels of *cyclin D1* are shown ($n = 3$ for each group; *** $p < 0.001$ by 2-way ANOVA followed by multiple comparison tests).

(E) Steady-state expression levels of *cyclin D1* in WT and mutant HOC313 cells expressing edited *cyclin D1* (Mut-*cyclin D1*) were examined by qPCR ($n = 3$ for each group; ** $p < 0.01$ by Student's *t* test).

(F) WT and mutant HOC313 cells expressing Mut-*cyclin D1* were transfected with the FUCCI plasmid. The duration of the G1 phase was calculated based on the duration of fluorescence ($n = 4$ for each group from independent experiments, ** $p < 0.01$ by Student's *t* test).

(G) Relative cell growth of WT and mutant HOC313 cells expressing Mut-*cyclin D1* ($n = 7$ – 8 for each group, *** $p < 0.001$, **** $p < 0.0001$ by 2-way ANOVA, followed by multiple comparison tests).

Data are presented as means \pm SEMs.

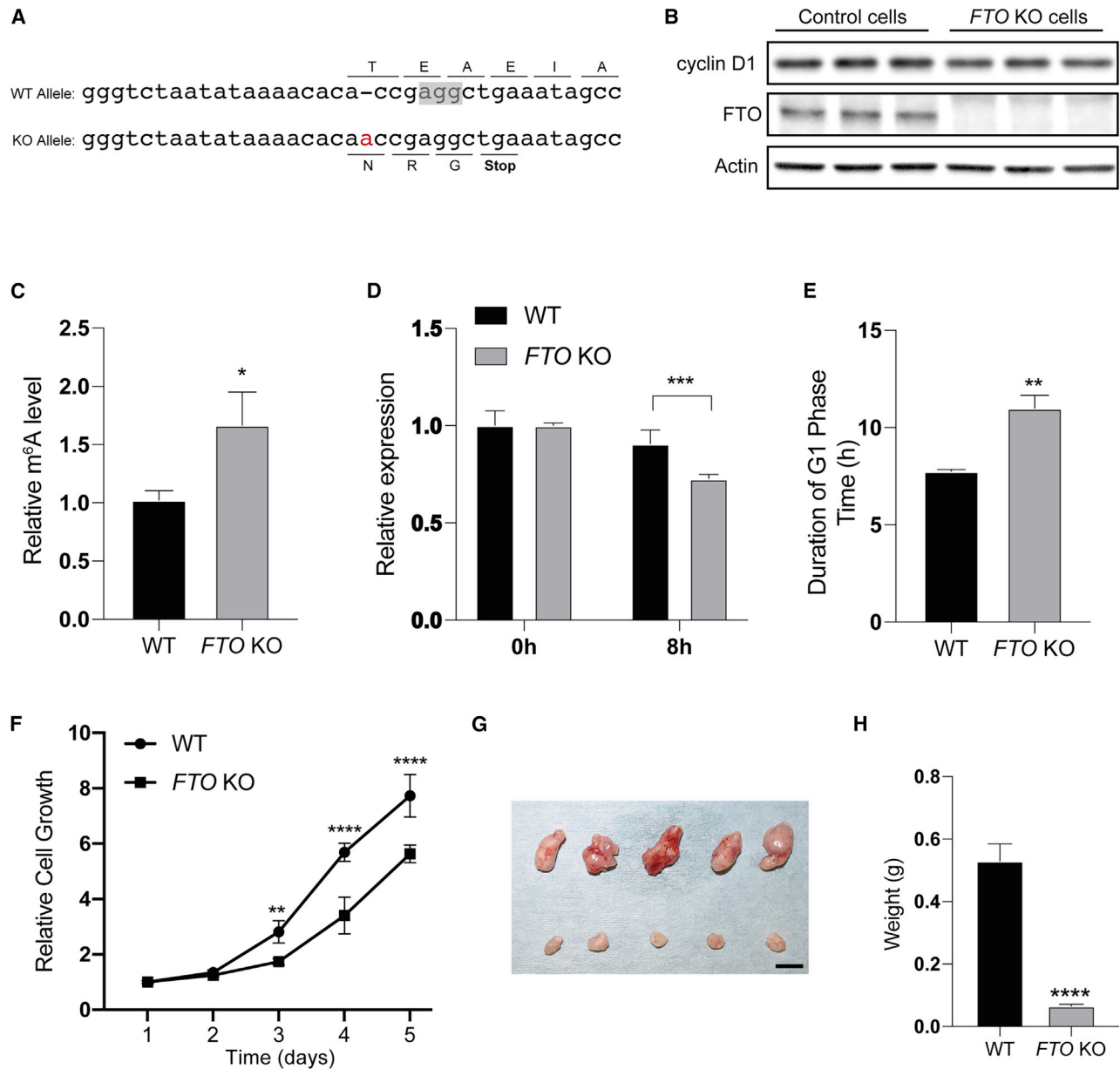


Figure 5. Loss of FTO1 Suppresses Cell Growth In Vivo

(A) Alignment of genomic sequences of WT and modified *FTO* genes (KO) edited by CRISPR-Cas9. The inserted nucleotide is highlighted in red. The PAM (protospacer adjacent motif) sequence is highlighted by a shaded box. Lines indicate the reading frame.

(B) Levels of cyclin D1 and FTO proteins examined by western blotting in WT and *FTO* KO SAS cells.

(C) The m⁶A level in the 5' UTR of *cyclin D1* was examined by MeRIP-qPCR. Note that the m⁶A level in *FTO* KO SAS cells is significantly higher than that in WT cells (n = 8–9 for each group; *p < 0.01 by Student's t test).

(D) WT and *FTO* KO SAS cells were treated with actinomycin D for 8 h, and the relative expression levels of *cyclin D1* are shown (n = 4 for each group; ***p < 0.001 by Student's t test).

(E) WT and *FTO* KO SAS cells were transfected with the FUCCI plasmid, and the duration of the G1 phase was calculated based on the duration of fluorescence (n = 4 for each group from independent experiments, **p < 0.01 by Student's t test).

(F) Relative cell growth of WT and *FTO* KO SAS cells (n = 4 for each group, **p < 0.01, ****p < 0.0001 by 2-way ANOVA, followed by multiple comparison tests).

(G) WT and *FTO* KO SAS cells were implanted in nude mice for 2 weeks. Solid tumors in mice were dissected and are shown. Bar, 1 cm.

(H) The weight of tumors (G) is shown. Note that the weight of tumors formed from *FTO* KO SAS cells is significantly lower than that of tumors formed from WT SAS cells. ****p < 0.0001 by Student's t test.

Data are presented as means ± SEMs.

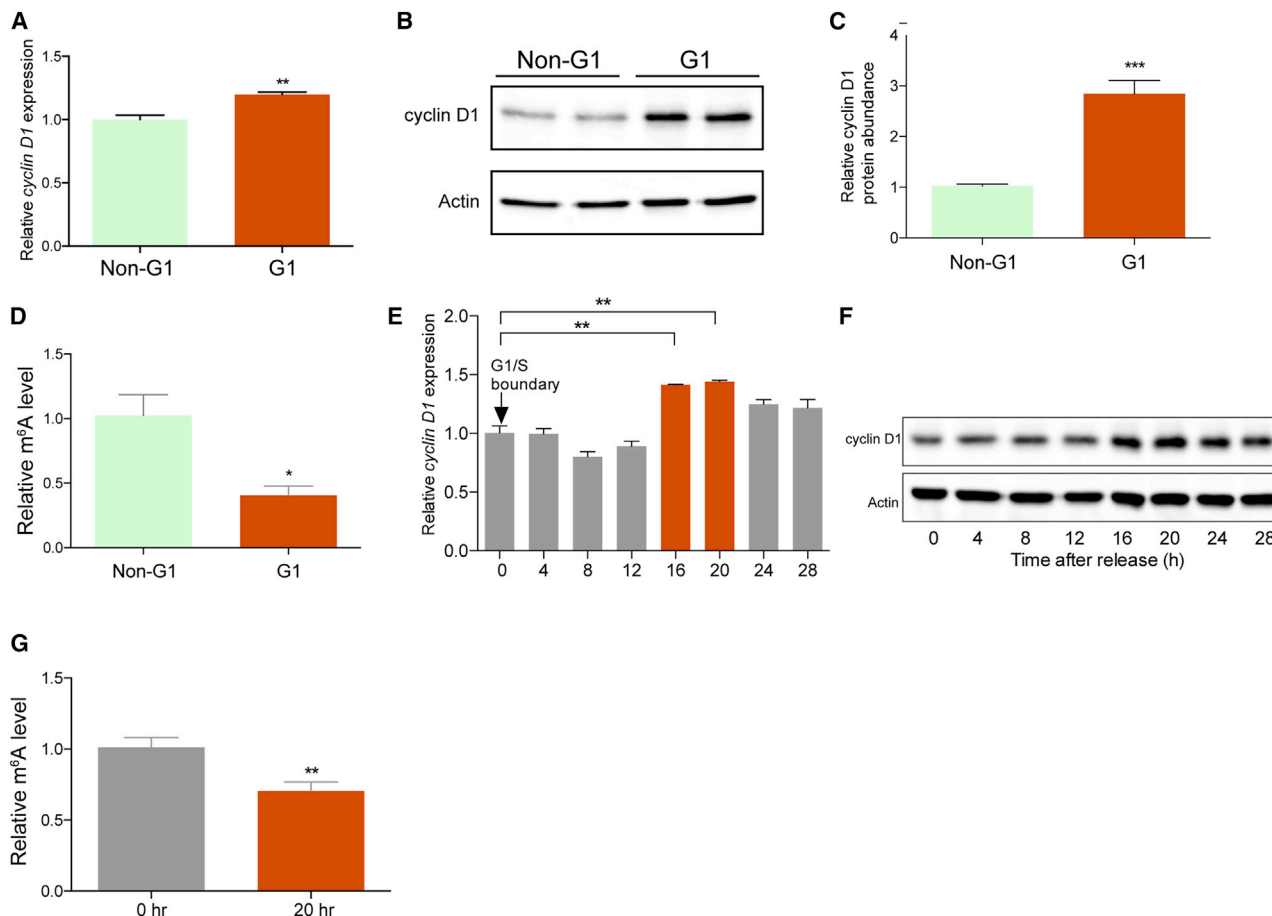


Figure 6. m⁶A Modification of Cyclin D1 Is Differentially Regulated during the Cell Cycle through Nucleocytoplasmic Shuttling of FTO

(A) FUCCI-expressing HOC313 cells at G1 and non-G1 (S/G2/M) phases were sorted by FACS. Cells at G1 display orange fluorescence and cells at non-G1 phases display green fluorescence. The relative expression level of *cyclin D1* in each cell-cycle phase was examined by qPCR (n = 3 for each group; *p < 0.05 by Student's t test).

(B) Cyclin D1 protein levels in G1 and non-G1 phases were examined in FUCCI-expressing HOC313 cells.

(C) Quantitation of cyclin D1 protein levels in G1 and non-G1 phase cells (n = 4 for non-G1 cells and n = 5 for G1 cells; ***p < 0.001 by Student's t test).

(D) m⁶A modification of *cyclin D1* in G1 and non-G1 phase cells was examined by MeRIP-qPCR (n = 3 for each group; *p < 0.05 by Student's t test).

(E) The cell cycle was synchronized at the G1-S phase boundary by thymidine treatment, and expression of *cyclin D1* was examined at the indicated time points after release of the cell cycle (**p < 0.01 by 1-way ANOVA, followed by multiple comparison tests).

(F) Cyclin D1 protein levels were examined by western blotting after release of the cell cycle.

(G) m⁶A modification of *cyclin D1* before (0 h) and after (20 h) release of the cell cycle, examined by MeRIP-qPCR (**p < 0.01 by Student's t test).

localization of the FTO 150E mutant failed to rescue the growth defect (cell growth at day 3: WT: 3.5 ± 0.22 , FTO KO: 1.7 ± 0.1 , FTO KO + FTO: 2.3 ± 0.14 , FTO KO + T150E: 1.8 ± 0.08 , FTO KO + T150A: 2.4 ± 0.27 ; Figure S6C).

Finally, we sought to identify the protein kinase responsible for the phosphorylation of FTO. Thr 4, Thr 6, and Thr 150 are surrounded by acidic amino acids within a predicted casein kinase II (CKII) recognition motif. CKII was found to be capable of phosphorylating FTO WT *in vitro* (Figure 7J). The degree of phosphorylation was decreased to 64% in T150A mutants compared with FTO WT (Figure 7J). Furthermore, the application of a CKII inhibitor (Inh) induced the nuclear localization of FTO (percentage of cells showing nuclear localization: vehicle: $38\% \pm 6.0\%$ versus CKII Inh: 100%; Figures 7K and S6D), which was associated with a significant decrease in the m⁶A level in *cyclin D1* (vehicle:

1.0 ± 0.09 versus CKII Inh: 0.37 ± 0.11 ; Figure 7L). These results suggest that CKII is involved in nucleocytoplasmic shuttling of FTO through phosphorylation at Thr 150.

DISCUSSION

In the present study, we discovered that FTO regulates the cell cycle by modulating the m⁶A modification of *cyclin D1*, the master regulator of G1 phase progression. FTO deficiency increased the m⁶A modification of *cyclin D1*, leading to the degradation of its mRNA. The loss of FTO significantly impaired cell proliferation in multiple cell lines, which could be rescued by FTO re-expression. Notably, FTO KO cells showed a marked growth defect in the mouse xenograft model. These results thus indicate that FTO is required for cell-cycle progression by controlling *cyclin*

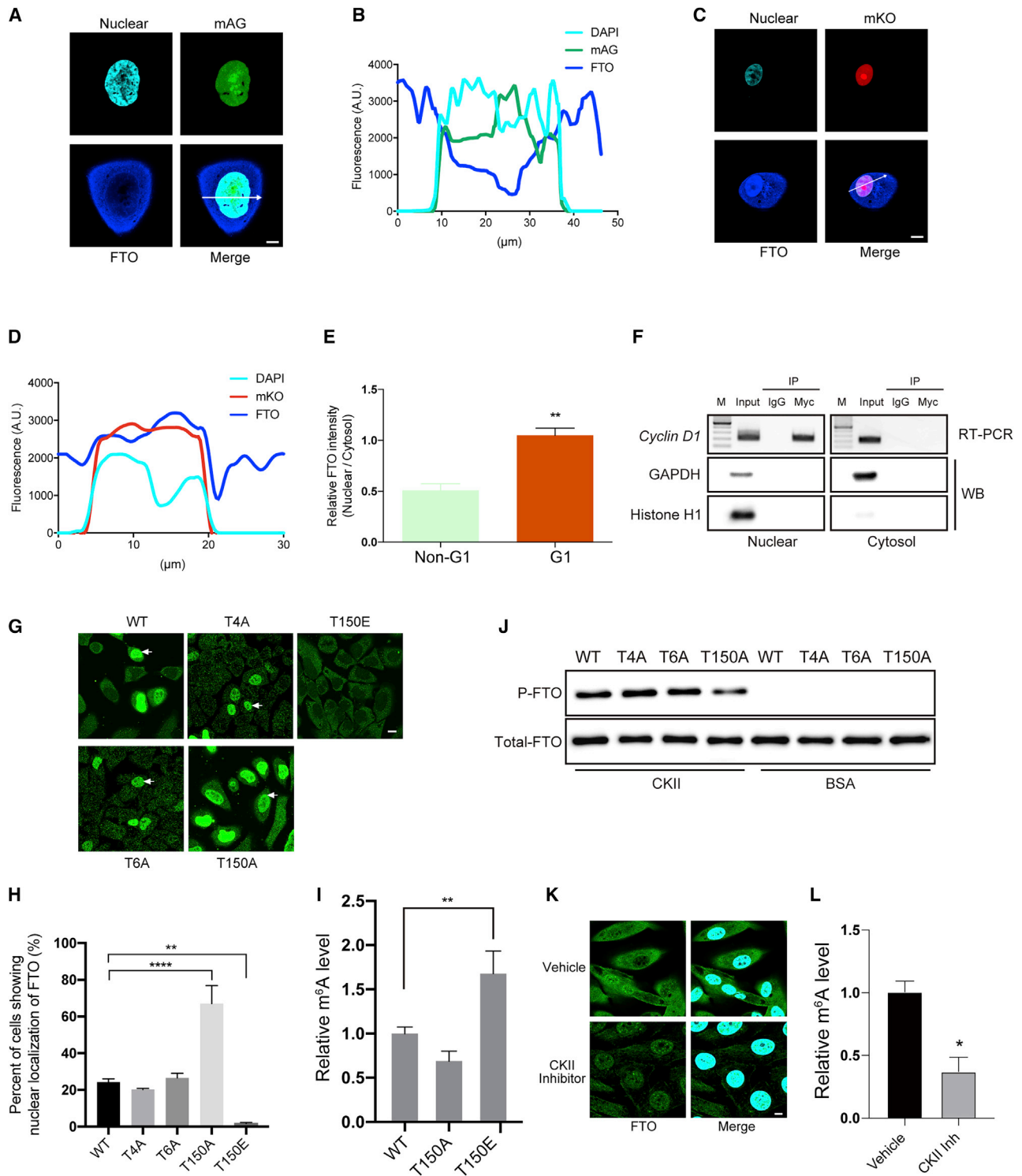


Figure 7. Regulation of FTO Nucleocytoplasmic Shuttling by Phosphorylation

(A) Representative FUCCI-expressing HOC313 cells in non-G1 phases. Bar, 10 μm .
(B) Fluorescence intensities of DAPI, mAG, and FTO along the white line in (A).
(C) Representative FUCCI-expressing HOC313 cells in the G1 phase. Bar, 10 μm .
(D) Fluorescence intensities of DAPI, mKO, and FTO along the white line in (C).

(legend continued on next page)

D1 mRNA. *FTO* is originally identified as a risk gene for obesity in genome-wide association studies (Scott et al., 2007; Scuteri et al., 2007). Multiple lines of *FTO* KO mice have been generated (Fischer et al., 2009; Church et al., 2009; Gao et al., 2010). These *FTO* KO mice showed postnatal growth retardation, which was associated with a decrease in fat and lean mass. Although dysregulation of energy expenditure was linked to the growth defect in *FTO* KO mice, a previous study has found a potential association between the decrease in the *cyclin D1* mRNA level and the impairment of mitotic clonal expansion of adipocytes in *FTO* KO mice (Merkestein et al., 2015). Thus, it is likely that dysregulation of the m⁶A modification of *cyclin D1* mRNA may contribute to the growth defect of *FTO* KO mice. Future study using *FTO* KO mice is needed to elucidate the potential roles of *cyclin D1* m⁶A modification *in vivo*.

Why *cyclin D1* mRNA needs to be regulated at the post-transcription level is an interesting question. During the transition of the cell cycle, elements belonging to the previous phase must be eliminated before or immediately after entry into the next phase, otherwise precise cell-cycle progression may be compromised. The molecular mechanism of the periodic regulation of *cyclin D1* has been extensively studied from a proteostatic standpoint. *Cyclin D1* levels start to rise early in the G1 phase, and the protein continues to accumulate in the nucleus throughout the G1 phase (Hydbring et al., 2016). At the G1-S phase boundary, *cyclin D1* is phosphorylated at threonine 286 (T286) by glycogen synthase kinase 3 β (GSK3 β), which facilitates its nuclear export and degradation by a ubiquitin-proteasome-mediated pathway (Diehl et al., 1998). In general, the steady-state level of any given protein, including *cyclin D1*, is determined by the balance of degradation and translation. Therefore, in addition to proteasomal degradation of the *cyclin D1* protein, removal of its mRNA is necessary to achieve maximal suppression. Although *cyclin D1* mRNA can be suppressed at the transcriptional level (Klein and Assoian, 2008), the molecular mechanism underlying the cell-cycle-specific destabilization of transcribed mRNA remains unclear. In the present study, we found that m⁶A modification of *cyclin D1* was minimal in the G1 phase, resulting in the stabilization of *cyclin D1* and upregulation of the gene product. By contrast, in non-G1 phases, m⁶A modification

of *cyclin D1* was extensive, which destabilized the mRNA and downregulated the gene product. In addition, we found that genetic elimination of m⁶A modification of the *cyclin D1* 5' UTR was sufficient to facilitate G1 progression. To our knowledge, this is the first report showing that post-transcriptional m⁶A modification of *cyclin D1* mRNA can undergo periodic changes during the cell cycle. Our results suggest that post-transcriptional m⁶A modification is involved in regulating the steady-state level of *cyclin D1* mRNA, which orchestrates with proteasome-mediated proteostatic regulation to ensure the optimal level of *cyclin D1* for precise cell-cycle progression.

It should be noted that *cyclin A*, *cyclin B1*, and *cyclin E* also show periodic changes during the cell cycle (Winston and Pledger, 1993; Desdouets et al., 1995; Polanowska et al., 2001). However, unlike *cyclin D1*, the mRNAs of these other *cyclins* contained only very low levels of m⁶A. In the present study, most cells were in the G1 phase, and only a small population of cells were in the non-G1 phases (Figure 1B). This bias in cell populations may cause an underestimation of m⁶A modification in *cyclin A*, *cyclin B1*, and *cyclin E*. The enrichment of cells at a specific cell-cycle phase is needed to verify whether m⁶A-mediated regulation is also preserved in these *non-D1 cyclins*. It is also worth mentioning that many m⁶A-containing genes can be targeted by *FTO* that are involved in cell-cycle progression besides *cyclin D1*. Future studies are needed to investigate other genes to understand the dynamic role of m⁶A modification during cell-cycle progression.

Our study revealed that m⁶A modification of *cyclin D1* is mediated by *FTO*. It is noteworthy that *FTO* is a demethylase for both m⁶A and N⁶, 2'-O-dimethyladenosine (m⁶Am), with a preference for m⁶Am over m⁶A under some conditions (Mauer et al., 2017; Wei et al., 2018). In vertebrate mRNA, when the transcription start nucleoside is adenosine, it is converted to m⁶Am by a cap-specific adenosine methyltransferase (CAPAM) (Akichika et al., 2019). The m⁶Am modification of mRNA is not related to mRNA stability, but it can promote translation. In the case of *cyclin D1*, the transcription start nucleoside appears to be cytidine (Matsushima et al., 1991). In addition, *cyclin D1* was not significantly downregulated in CAPAM KO HeLa cells. These observations suggest that *FTO*-mediated demethylation of m⁶Am is not

(E) *FTO* intensity in the nucleus in the G1 phase is higher than that in non-G1 phases (n = 6 for non-G1 phase cells, n = 7 for G1 phase cells; **p < 0.01 by Mann-Whitney test).

(F) HeLa cells were transfected with Myc-*FTO*, followed by UV crosslinking and fractionation of nuclear and cytosolic fractions. The *FTO*-RNA complex in each fraction was immunoprecipitated using control IgG or anti-Myc antibody. *FTO*-bound *cyclin D1* was detected by RT-PCR. Western blotting using antibodies against glyceraldehyde 3-phosphate dehydrogenase (GAPDH) and histone H1 was performed to confirm the purity of cytosol and nuclear fractions, respectively. Three independent experiments were performed, and representative images are shown.

(G) *FTO* WT, *FTO* T4A, *FTO* T6A, and *FTO* T150A were conjugated to a Myc-tag at the C terminus and transfected into HeLa cells. HeLa cells were immunostained with anti-Myc antibody to visualize exogenous *FTO*. Representative images of HeLa cells expressing each type of *FTO* are shown. Arrows indicate the nuclear localization of *FTO*. Bar, 10 μ m.

(H) Percentage of cells showing nuclear localization of WT *FTO*, T4A *FTO*, T6A *FTO*, T150A *FTO*, and T150E *FTO* (n = 4–7 biological replicates for each group; **p < 0.01, ***p < 0.001 by 1-way ANOVA).

(I) m⁶A modification of *cyclin D1* in cells expressing *FTO* WT, *FTO* T150A, or *FTO* T150E examined by MeRIP-qPCR (n = 9 for WT, n = 7 for T150A, n = 5 for T150E; **p < 0.01 by 1-way ANOVA).

(J) Recombinant glutathione S-transferase (GST)-tagged *FTO* (WT, T4A, T6A, or T150A) was purified and subjected to *in vitro* phosphorylation by CKII. Phosphorylated *FTO* (P-*FTO*) was detected by anti-thiophosphate-ester antibody, and the total amount of each type of *FTO* was measured by anti-*FTO* antibody.

(K) HOC313 cells were incubated with 1 μ M CKII inhibitor for 24 h and immunostained with anti-*FTO* antibody. Bar, 10 μ m.

(L) m⁶A modification of *cyclin D1* in HOC313 cells treated with vehicle or CKII inhibitor examined by MeRIP-qPCR (n = 4 for each group; *p < 0.01 by Student's t test).

Data are presented as means \pm SEMs.

involved in the regulation of *cyclin D1*. One major limitation of the current MeRIP-seq method is that the m⁶A antibody cannot distinguish between m⁶A and m⁶Am. Future studies using CA-PAM KO cells are therefore required to dissociate the effects of m⁶A from those of m⁶Am.

In the present study, we found that oscillation of m⁶A modification was associated with differential cellular localization of FTO, but not with FTO mRNA or protein levels. In the G1 phase, FTO is enriched in the nucleus, and this is associated with decreased m⁶A modification of *cyclin D1*. By contrast, FTO is enriched in the cytosol in non-G1 phases, and this is associated with increased m⁶A modification of *cyclin D1*. Notably, we found that nuclear FTO is bound to *cyclin D1* mRNA, while cytosolic FTO does not interact with *cyclin D1*. These results suggest that FTO is not capable of demethylating *cyclin D1* once it is exported to cytosol. Although FTO appears to be preferentially localized in the nucleus, previous studies showed that FTO is capable of localizing to the cytosol, and even shuttling between the nucleus and cytosol (Aas et al., 2017; Landfors et al., 2016; Vujovic et al., 2013; Gulati et al., 2014). However, the molecular mechanism underlying the nucleocytoplasmic shuttling of FTO is largely unexplored. In the present study, we provide evidence that the shuttling of FTO may be regulated by a CKII-mediated phosphorylation. CKII is a serine/threonine kinase that is required for progression from the G1 phase to the S phase (Russo et al., 1992). We showed that CKII can phosphorylate FTO at Thr 150, and this triggers the export of FTO from the nucleus to the cytosol, leading to an increase in m⁶A modification of *cyclin D1*. Transient expression of WT and nuclear-localizing FTO 150A mutants partially rescued the growth defect of FTO-deficient cells, while the expression of cytosol-localizing FTO 150E did not demonstrate a rescuing effect in FTO-deficient cells. Thus, it is conceivable that the CKII-FTO axis is responsible for cell-cycle progression from the G1 phase to the S phase by regulating FTO localization. Our results reveal dynamic crosstalk between epitranscriptomic and post-translational regulation of the cell cycle. It should be noted that the rescuing effect of FTO 150A mutant only became obvious on the second day, not the first day, after the transfection of plasmids. This slow rescuing effect may be attributed to the time lag in the accumulation of sufficient exogenous FTO mutants after transfection, which normally requires 24 h to achieve maximum expression. A limitation of the present study is that many experiments were performed by overexpressing the FTO gene. Although the exogenous Myc-tagged FTO enables better detection and efficient immunoprecipitation, whether endogenous FTO is regulated by the same mechanisms needs to be elucidated. Editing the endogenous *FTO* gene by CRISPR-Cas9 or generating phosphorylation-specific antibodies is needed in the future study.

In addition to FTO, ALKBH5 also demethylates m⁶A and is involved in regulating cell differentiation and proliferation. A recent study showed that ALKBH5 contributes to tumorigenicity in glioblastoma stem-like cells (GSCs) by demethylating *Forkhead box protein M1 (FOXM1)*, an important regulator of cell proliferation (Zhang et al., 2017). The loss of *ALKBH5* function increased the m⁶A modification of *FOXM1*, leading to the degradation of its mRNA and the suppressed growth of GSCs. *Cyclin D1* was not a direct target of ALKBH5 in the study. Therefore, it is

likely that ALKBH5 and FTO differentially demethylate cell-cycle-related genes and contribute to cell-cycle progression in concert.

In summary, our results suggest that cell-cycle progression is in part controlled by the dynamic oscillation of m⁶A modification of mRNAs, regulated by FTO. These findings highlight the importance of epitranscriptomic regulation of gene expression during the cell cycle.

STAR★METHODS

Detailed methods are provided in the online version of this paper and include the following:

- KEY RESOURCES TABLE
- LEAD CONTACT AND MATERIALS AVAILABILITY
- EXPERIMENTAL MODEL AND SUBJECT DETAILS
 - Mice
 - Cell lines
- METHOD DETAILS
 - Transfection of siRNAs
 - Cell growth assay
 - Construction of a Fucci-expressing cell line
 - Time-lapse imaging of the cell cycle
 - Sorting of Fucci-expressing cells
 - Cell cycle analysis by double thymidine blocking
 - Gene editing by CRISPR/Cas9
 - Immunocytochemistry and confocal imaging
 - RNA stability assay
 - Quantitative PCR
 - Protein extraction and western blotting
 - Dot blot analysis
 - LC-MS/MS
 - RNA-seq
 - MeRIP-seq
 - MeRIP-qPCR
 - Purification of FTO protein
 - Kinase assay
 - Construction of siRNA- and CRISPR-insensitive human FTO
 - Immunoprecipitation of the FTO-RNA complex
 - Xenograft model
 - Data analysis
- QUANTIFICATION AND STATISTICAL ANALYSIS
- DATA AND CODE AVAILABILITY

SUPPLEMENTAL INFORMATION

Supplemental Information can be found online at <https://doi.org/10.1016/j.celrep.2020.03.028>.

ACKNOWLEDGMENTS

We thank Dr. Shinjiro Hino (Kumamoto University) for advice regarding the data analysis and Ms. Nobuko Maeda and Dr. Toshiro Moroishi for technical assistance. We thank Dr. Shuichi Kawashiri and Dr. Koroku Kato (Department of Oral and Maxillofacial Surgery, Kanazawa University Graduate School of Medical Science, Ishikawa 920-8641, Japan) for providing the HOC313 cells. This work was supported by Grants-in-Aid for Scientific Research from the Ministry of Education, Culture, Sports, Sciences, and Technology of Japan

(17905074 and 18959602 to K.T.; 18H02599 and 18K19521 to F.-Y.W.), the Japan Agency for Medical Research and Development (AMED; 17935694 to K.T.), the Takeda Science Foundation (to K.T.), and the Japan Science and Technology Agency (JST; to F.-Y.W. and S.O.).

AUTHOR CONTRIBUTIONS

M.H., M.Y., and N.T. performed the experiments. S.O. performed the data analysis. R.Y. and H.N. prepared the cell lines. F.-Y.W., T.C., and K.T. designed the experiments. M.H., F.-Y.W., and K.T. wrote the manuscript.

DECLARATION OF INTERESTS

The authors declare no competing interests.

Received: July 8, 2019

Revised: January 14, 2020

Accepted: March 11, 2020

Published: April 7, 2020

REFERENCES

- Aas, A., Isakson, P., Bindesbøll, C., Alemu, E.A., Klungland, A., and Simonsen, A. (2017). Nucleocytoplasmic shuttling of FTO does not affect starvation-induced autophagy. *PLoS One* *12*, e0168182.
- Afgan, E., Baker, D., Batut, B., van den Beek, M., Bouvier, D., Cech, M., Chilton, J., Clements, D., Coraor, N., Grünig, B.A., et al. (2018). The Galaxy platform for accessible, reproducible and collaborative biomedical analyses: 2018 update. *Nucl. Acids Res.* *46*, W537–W544.
- Akichika, S., Hirano, S., Shichino, Y., Suzuki, T., Nishimasu, H., Ishitani, R., Sugita, A., Hirose, Y., Iwasaki, S., Nureki, O., and Suzuki, T. (2019). Cap-specific terminal N⁶-methylation of RNA by an RNA polymerase II-associated methyltransferase. *Science* *363*, 141.
- Baldin, V., Lukas, J., Marcote, M.J., Pagano, M., and Draetta, G. (1993). Cyclin D1 is a nuclear protein required for cell cycle progression in G1. *Genes Dev.* *7*, 812–821.
- Bertoli, C., Skotheim, J.M., and de Bruin, R.A. (2013). Control of cell cycle transcription during G1 and S phases. *Nat. Rev. Mol. Cell Biol.* *14*, 518–528.
- Boissel, S., Reish, O., Proulx, K., Kawagoe-Takaki, H., Sedgwick, B., Yeo, G.S., Meyre, D., Golzio, C., Molinari, F., Kadhom, N., et al. (2009). Loss-of-function mutation in the dioxygenase-encoding FTO gene causes severe growth retardation and multiple malformations. *Am. J. Hum. Genet.* *85*, 106–111.
- Church, C., Lee, S., Bagg, E.A., McTaggart, J.S., Deacon, R., Gerken, T., Lee, A., Moir, L., Mecinović, J., Quwailid, M.M., et al. (2009). A mouse model for the metabolic effects of the human fat mass and obesity associated FTO gene. *PLoS Genet.* *5*, e1000599.
- Desdouets, C., Matesic, G., Molina, C.A., Foulkes, N.S., Sassone-Corsi, P., Brechot, C., and Sobczak-Thépot, J. (1995). Cell cycle regulation of cyclin A gene expression by the cyclic AMP-responsive transcription factors CREB and CREM. *Mol. Cell. Biol.* *15*, 3301–3309.
- Diehl, J.A., Cheng, M., Roussel, M.F., and Sherr, C.J. (1998). Glycogen synthase kinase-3 β regulates cyclin D1 proteolysis and subcellular localization. *Genes Dev.* *12*, 3499–3511.
- Dominissini, D., Moshitch-Moshkovitz, S., Schwartz, S., Salmon-Divon, M., Ungar, L., Osenberg, S., Cesarkas, K., Jacob-Hirsch, J., Amariglio, N., Kupiec, M., et al. (2012). Topology of the human and mouse m6A RNA methylomes revealed by m6A-seq. *Nature* *485*, 201–206.
- Fasanaro, P., Capogrossi, M.C., and Martelli, F. (2010). Regulation of the endothelial cell cycle by the ubiquitin-proteasome system. *Cardiovasc. Res.* *85*, 272–280.
- Fischer, J., Koch, L., Emmerling, C., Vierkotten, J., Peters, T., Brüning, J.C., and Rüther, U. (2009). Inactivation of the Fto gene protects from obesity. *Nature* *458*, 894–898.
- Fu, Y., Jia, G., Pang, X., Wang, R.N., Wang, X., Li, C.J., Smemo, S., Dai, Q., Bailey, K.A., Nobrega, M.A., et al. (2013). FTO-mediated formation of N⁶-hydroxymethyladenosine and N⁶-formyladenosine in mammalian RNA. *Nat. Commun.* *4*, 1798.
- Fu, Y., Dominissini, D., Rechavi, G., and He, C. (2014). Gene expression regulation mediated through reversible m⁶A RNA methylation. *Nat. Rev. Genet.* *15*, 293–306.
- Fustin, J.M., Doi, M., Yamaguchi, Y., Hida, H., Nishimura, S., Yoshida, M., Isagawa, T., Morioka, M.S., Kakeya, H., Manabe, I., and Okamura, H. (2013). RNA-methylation-dependent RNA processing controls the speed of the circadian clock. *Cell* *155*, 793–806.
- Gao, X., Shin, Y.H., Li, M., Wang, F., Tong, Q., and Zhang, P. (2010). The fat mass and obesity associated gene FTO functions in the brain to regulate post-natal growth in mice. *PLoS One* *5*, e14005.
- Gulati, P., Avezov, E., Ma, M., Antrobus, R., Lehner, P., O'Rahilly, S., and Yeo, G.S.H. (2014). Fat mass and obesity-related (FTO) shuttles between the nucleus and cytoplasm. *Biosci. Rep.* *34*, 621–628.
- Han, Z., Niu, T., Chang, J., Lei, X., Zhao, M., Wang, Q., Cheng, W., Wang, J., Feng, Y., and Chai, J. (2010). Crystal structure of the FTO protein reveals basis for its substrate specificity. *Nature* *464*, 1205–1209.
- Hsu, P.J., Zhu, Y., Ma, H., Guo, Y., Shi, X., Liu, Y., Qi, M., Lu, Z., Shi, H., Wang, J., et al. (2017). Ythdc2 is an N⁶-methyladenosine binding protein that regulates mammalian spermatogenesis. *Cell Res.* *27*, 1115–1127.
- Hydbring, P., Malumbres, M., and Sicinski, P. (2016). Non-canonical functions of cell cycle cyclins and cyclin-dependent kinases. *Nat. Rev. Mol. Cell Biol.* *17*, 280–292.
- Jia, G., Fu, Y., Zhao, X., Dai, Q., Zheng, G., Yang, Y., Yi, C., Lindahl, T., Pan, T., Yang, Y.G., and He, C. (2011). N⁶-methyladenosine in nuclear RNA is a major substrate of the obesity-associated FTO. *Nat. Chem. Biol.* *7*, 885–887.
- Ke, S., Pandya-Jones, A., Saito, Y., Fak, J.J., Vågbo, C.B., Geula, S., Hanna, J.H., Black, D.L., Darnell, J.E., Jr., and Darnell, R.B. (2017). m⁶A mRNA modifications are deposited in nascent pre-mRNA and are not required for splicing but do specify cytoplasmic turnover. *Genes Dev.* *31*, 990–1006.
- Klein, E.A., and Assoian, R.K. (2008). Transcriptional regulation of the cyclin D1 gene at a glance. *J. Cell Sci.* *121*, 3853–3857.
- Landfors, M., Nakken, S., Fusser, M., Dahl, J.A., Klungland, A., and Fedorcsak, P. (2016). Sequencing of FTO and ALKBH5 in men undergoing infertility work-up identifies an infertility-associated variant and two missense mutations. *Fertil. Steril.* *105*, 1170–1179.e5.
- Li, A., Chen, Y.S., Ping, X.L., Yang, X., Xiao, W., Yang, Y., Sun, H.Y., Zhu, Q., Baidya, P., Wang, X., et al. (2017a). Cytoplasmic m⁶A reader YTHDF3 promotes mRNA translation. *Cell Res.* *27*, 444–447.
- Li, Z., Weng, H., Su, R., Weng, X., Zuo, Z., Li, C., Huang, H., Nachtergaele, S., Dong, L., Hu, C., et al. (2017b). FTO plays an oncogenic role in acute myeloid leukemia as a N⁶-methyladenosine RNA demethylase. *Cancer Cell* *31*, 127–141.
- Lim, S., and Kaldis, P. (2013). Cdks, cyclins and CKIs: roles beyond cell cycle regulation. *Development* *140*, 3079–3093.
- Lin, D.I., Barbash, O., Kumar, K.G.S., Weber, J.D., Harper, J.W., Klein-Szanto, A.J.P., Rustgi, A., Fuchs, S.Y., and Diehl, J.A. (2006). Phosphorylation-dependent ubiquitination of cyclin D1 by the SCF(FBX4- α -crystallin) complex. *Mol. Cell* *24*, 355–366.
- Liu, J., Yue, Y., Han, D., Wang, X., Fu, Y., Zhang, L., Jia, G., Yu, M., Lu, Z., Deng, X., et al. (2014). A METTL3-METTL14 complex mediates mammalian nuclear RNA N⁶-adenosine methylation. *Nat. Chem. Biol.* *10*, 93–95.
- Liu, Y., Chen, S., Wang, S., Soares, F., Fischer, M., Meng, F., Du, Z., Lin, C., Meyer, C., DeCaprio, J.A., et al. (2017). Transcriptional landscape of the human cell cycle. *Proc. Natl. Acad. Sci. USA* *114*, 3473–3478.
- Marumoto, T., Tashiro, A., Friedmann-Morvinski, D., Scadeng, M., Soda, Y., Gage, F.H., and Verma, I.M. (2009). Development of a novel mouse glioma model using lentiviral vectors. *Nat. Med.* *15*, 110–116.

- Matsushime, H., Roussel, M.F., Ashmun, R.A., and Sherr, C.J. (1991). Colony-stimulating factor 1 regulates novel cyclins during the G1 phase of the cell cycle. *Cell* 65, 701–713.
- Mauer, J., Luo, X., Blanjoie, A., Jiao, X., Grozhik, A.V., Patil, D.P., Linder, B., Pickering, B.F., Vasseur, J.J., Chen, Q., et al. (2017). Reversible methylation of m⁶A_m in the 5' cap controls mRNA stability. *Nature* 541, 371–375.
- Mendel, M., Chen, K.M., Homolka, D., Gos, P., Pandey, R.R., McCarthy, A.A., and Pillai, R.S. (2018). Methylation of structured RNA by the m6A writer METTL16 is essential for mouse embryonic development. *Mol. Cell* 71, 986–1000.e11.
- Merkestein, M., Laber, S., McMurray, F., Andrew, D., Sachse, G., Sanderson, J., Li, M., Usher, S., Sellayah, D., Ashcroft, F.M., and Cox, R.D. (2015). FTO influences adipogenesis by regulating mitotic clonal expansion. *Nat. Commun.* 6, 6792.
- Meyer, K.D., and Jaffrey, S.R. (2014). The dynamic epitranscriptome: N6-methyladenosine and gene expression control. *Nat. Rev. Mol. Cell Biol.* 15, 313–326.
- Ping, X.L., Sun, B.F., Wang, L., Xiao, W., Yang, X., Wang, W.J., Adhikari, S., Shi, Y., Lv, Y., Chen, Y.S., et al. (2014). Mammalian WTAP is a regulatory subunit of the RNA N6-methyladenosine methyltransferase. *Cell Res.* 24, 177–189.
- Polanowska, J., Fabrizio, E., Le Cam, L., Trouche, D., Emiliani, S., Herrera, R., and Sardet, C. (2001). The periodic down regulation of cyclin E gene expression from exit of mitosis to end of G(1) is controlled by a deacetylase- and E2F-associated bipartite repressor element. *Oncogene* 20, 4115–4127.
- Russo, G.L., Vandenberg, M.T., Yu, I.J., Bae, Y.S., Franza, B.R., Jr., and Marshak, D.R. (1992). Casein kinase II phosphorylates p34cdc2 kinase in G1 phase of the HeLa cell division cycle. *J. Biol. Chem.* 267, 20317–20325.
- Sakaue-Sawano, A., Kurokawa, H., Morimura, T., Hanyu, A., Hama, H., Osawa, H., Kashiwagi, S., Fukami, K., Miyata, T., Miyoshi, H., et al. (2008). Visualizing spatiotemporal dynamics of multicellular cell-cycle progression. *Cell* 132, 487–498.
- Sanjana, N.E., Shalem, O., and Zhang, F. (2014). Improved vectors and genome-wide libraries for CRISPR screening. *Nat. Methods* 11, 783–784.
- Satoh, T., and Kaida, D. (2016). Upregulation of p27 cyclin-dependent kinase inhibitor and a C-terminus truncated form of p27 contributes to G1 phase arrest. *Sci. Rep.* 6, 27829.
- Scott, L.J., Mohlke, K.L., Bonnycastle, L.L., Willer, C.J., Li, Y., Duren, W.L., Erdos, M.R., Stringham, H.M., Chines, P.S., Jackson, A.U., et al. (2007). A genome-wide association study of type 2 diabetes in Finns detects multiple susceptibility variants. *Science* 316, 1341–1345.
- Scuteri, A., Sanna, S., Chen, W.M., Uda, M., Albai, G., Strait, J., Najjar, S., Nagaraja, R., Orrù, M., Usala, G., et al. (2007). Genome-wide association scan shows genetic variants in the FTO gene are associated with obesity-related traits. *PLoS Genet.* 3, e115.
- Tang, C., Klukovich, R., Peng, H., Wang, Z., Yu, T., Zhang, Y., Zheng, H., Klungland, A., and Yan, W. (2018). ALKBH5-dependent m⁶A demethylation controls splicing and stability of long 3'-UTR mRNAs in male germ cells. *Proc. Natl. Acad. Sci. USA* 115, E325–E333.
- Vujovic, P., Stamenkovic, S., Jasnic, N., Lacic, I., Djurasevic, S.F., Cvijic, G., and Djordjevic, J. (2013). Fasting induced cytoplasmic Fto expression in some neurons of rat hypothalamus. *PLoS One* 8, e63694.
- Wang, X., Lu, Z., Gomez, A., Hon, G.C., Yue, Y., Han, D., Fu, Y., Parisien, M., Dai, Q., Jia, G., et al. (2014). N6-methyladenosine-dependent regulation of messenger RNA stability. *Nature* 505, 117–120.
- Wang, X., Zhao, B.S., Roundtree, I.A., Lu, Z., Han, D., Ma, H., Weng, X., Chen, K., Shi, H., and He, C. (2015). N(6)-methyladenosine Modulates Messenger RNA Translation Efficiency. *Cell* 161, 1388–1399.
- Wei, J., Liu, F., Lu, Z., Fei, Q., Ai, Y., He, P.C., Shi, H., Cui, X., Su, R., Klungland, A., et al. (2018). Differential m6A, m6Am, and m1A demethylation mediated by FTO in the cell nucleus and cytoplasm. *Mol. Cell* 71, 973–985.e5.
- Winston, J.T., and Pledger, W.J. (1993). Growth factor regulation of cyclin D1 mRNA expression through protein synthesis-dependent and -independent mechanisms. *Mol. Biol. Cell* 4, 1133–1144.
- Wojtas, M.N., Pandey, R.R., Mendel, M., Homolka, D., Sachidanandam, R., and Pillai, R.S. (2017). Regulation of m⁶A Transcripts by the 3'→5' RNA Helicase YTHDC2 Is Essential for a Successful Meiotic Program in the Mammalian Germline. *Mol. Cell* 68, 374–387.e12.
- Wu, R., Liu, Y., Yao, Y., Zhao, Y., Bi, Z., Jiang, Q., Liu, Q., Cai, M., Wang, F., Wang, Y., and Wang, X. (2018). FTO regulates adipogenesis by controlling cell cycle progression via m⁶A-YTHDF2 dependent mechanism. *Biochim. Biophys. Acta Mol. Cell. Biol. Lipids* 1863, 1323–1330.
- Xiao, W., Adhikari, S., Dahal, U., Chen, Y.S., Hao, Y.J., Sun, B.F., Sun, H.Y., Li, A., Ping, X.L., Lai, W.Y., et al. (2016). Nuclear m(6)A Reader YTHDC1 Regulates mRNA Splicing. *Mol. Cell* 61, 507–519.
- Xu, D., Shao, W., Jiang, Y., Wang, X., Liu, Y., and Liu, X. (2017). FTO expression is associated with the occurrence of gastric cancer and prognosis. *Oncol. Rep.* 38, 2285–2292.
- Zhang, S., Zhao, B.S., Zhou, A., Lin, K., Zheng, S., Lu, Z., Chen, Y., Sulman, E.P., Xie, K., Bögl, O., et al. (2017). m⁶A Demethylase ALKBH5 Maintains Tumorigenicity of Glioblastoma Stem-like Cells by Sustaining FOXM1 Expression and Cell Proliferation Program. *Cancer Cell* 31, 591–606.e6.
- Zhao, X., Yang, Y., Sun, B.F., Shi, Y., Yang, X., Xiao, W., Hao, Y.J., Ping, X.L., Chen, Y.S., Wang, W.J., et al. (2014). FTO-dependent demethylation of N6-methyladenosine regulates mRNA splicing and is required for adipogenesis. *Cell Res.* 24, 1403–1419.
- Zhao, B.S., Roundtree, I.A., and He, C. (2017). Post-transcriptional gene regulation by mRNA modifications. *Nat. Rev. Mol. Cell Biol.* 18, 31–42.
- Zheng, G., Dahl, J.A., Niu, Y., Fedorcsak, P., Huang, C.M., Li, C.J., Vågbo, C.B., Shi, Y., Wang, W.L., Song, S.H., et al. (2013). ALKBH5 is a mammalian RNA demethylase that impacts RNA metabolism and mouse fertility. *Mol. Cell* 49, 18–29.
- Zhu, T., Roundtree, I.A., Wang, P., Wang, X., Wang, L., Sun, C., Tian, Y., Li, J., He, C., and Xu, Y. (2014). Crystal structure of the YTH domain of YTHDF2 reveals mechanism for recognition of N6-methyladenosine. *Cell Res.* 24, 1493–1496.

STAR★METHODS

KEY RESOURCES TABLE

REAGENT or RESOURCE	SOURCE	IDENTIFIER
Antibodies		
m ⁶ A(N ⁶ -methyladenosine) antibody	Synaptic Systems	Cat#202003; RRID: AB_2279214
Anti-FTO antibody(5-2H10)	Abcam	Cat#ab92821; RRID: AB_10565042
Cyclin D1(DCS6) Mouse mAb	Cell Signaling Technology	Cat#2926; RRID: AB_2070400
Anti-Myc-tag-mAb	MBL	Cat#M047-3; RRID: AB_11160947
Anti-Thiophosphate ester	Abcam	Cat#ab92570; RRID: AB_10562142
Normal Rabbit IgG	Cell Signaling Technology	Cat#2729S; RRID: AB_1031062
Anti-B-Actin mAb	MBL international	Cat#M177-3; RRID: AB_10697039
Goat anti-Rabbit IgG(H+L) Secondary Antibody, HRP	Invitrogen	Cat#31460; RRID: AB_228341
Polyclonal Goat Anti-Mouse Immunoglobulins antibody	Dako	Cat#P0447; RRID: AB_2617137
Bacterial and Virus Strains		
lentiCRISPR v2	Sanjana et al., 2014	Addgene, Cat#52961
BL21 (DE3) Competent E.coli	New England Biolabs	Cat#C2527H
Chemicals, Peptides, and Recombinant Proteins		
Lipofectamine RNAiMAX transfection reagent	Invitrogen	Cat#13778075
Lipofectamine 2000	Invitrogen	Cat#11668019
Lipofectamine 3000	Invitrogen	Cat#L3000015
PrimeScript RT Master Mix (Perfect Real Time)	TAKARA	Cat#RR036A
TB Green Premix Ex TaqII	TAKARA	Cat#RR820A
Cell Counting Kit-8	Dojindo	Cat#347-07621
Dynabeads Protein G	Invitrogen	Cat#10003D
Actinomycin D	Fujifilm Wako	Cat#014-21261
Thymidine	Nacalai Tesque	Cat#07147-61
4',6-Diamidine-2'-phenylindole dihydrochloride	Roche	Cat#10236276001
Recombinant FTO protein	Active motif	Cat#31572
InSolution Casein Kinase II Inhibitor -Calbiochem	Merck	Cat#218708-5MGCN
Casein Kinase II (CK2)	New England BioLabs	Cat#P6010S
Adenosine 5'-[γ-thio] triphosphate tetralithium salt	Sigma	Cat#A1388
p-Nitrobenzyl mesylate. Alkylation reagent	Abcam	Cat#ab138910
Critical Commercial Assays		
Oligotex TM-dt30 < super > mRNA purification kit	TAKARA	Cat#9086
Cell Counting Kit-8	Dojindo	341-07761
Deposited Data		
RNA-seq data	This study	GSE133857
Experimental Models: Cell Lines		
HOC313	A gift from Drs. Shuichi Kawashiri and Koroku Kato	N/A
HeLa	ATCC	Cat#CCL-2
SAS	JCRB Cell Bank	JCRB0260
MDA-MB-231	ATCC	HTB-26
293FT	Thermo Fisher	R70007
MKN45	JCRB Cell Bank	JCRB0254

(Continued on next page)

Continued

REAGENT or RESOURCE	SOURCE	IDENTIFIER
Experimental Models: Mouse		
BALB/c-nu	Charles River Laboratories	N/A
Oligonucleotides		
Stealth siFTO#1	Invitrogen	Cat#1299001, HSS187971
Stealth siFTO#2	Invitrogen	Cat#1299001, HSS187970
Silencer TM Select Negative Control	Invitrogen	Cat#4390843
See Table S1 for primer sequences	This paper	N/A
Recombinant DNA		
pFucci-G1 Orange (Cloning vector)	Amalgaam	Cat#AM-V9001M
pFucci-S/G2/M Green (Cloning vector)	Amalgaam	Cat#AM-V9014M
pTomo	Marumoto et al., 2009	Addgene Cat#26291
psPAX2	Trono Lab Packaging and Envelope Plasmids (unpublished data)	Addgene Cat#12260
pMD2.G	Trono Lab Packaging and Envelope Plasmids (unpublished data)	Addgene Cat#12259
pGEX4T1	GE Healthcare	28954549
pEGFP-N1	Clontech	N/A
Human FTO cDNA	This Study	N/A
Software and Algorithms		
Prism8	GraphPad	N/A
Galaxy	Afgan et al. (2018)	https://usegalaxy.org

LEAD CONTACT AND MATERIALS AVAILABILITY

Further information and requests for resources and reagents should be directed to and will be fulfilled by the Lead Contact Fan-Yan Wei (fanyan.wei.d3@tohoku.ac.jp). This study did not generate new unique reagents.

EXPERIMENTAL MODEL AND SUBJECT DETAILS

Mice

For xenografting human cells, this study utilized murine animal models, consisting of 7-week-old male BALB/c-nu (CAnN.Cg-Foxn1nu/CrlCr) mice purchased from Charles River Laboratories. All mice were housed in groups of 4~5 in plastic cages at 25°C with 12-h light and 12-h dark cycles and free access to water and food until 7-week-old. Mice were randomly divided into two groups: one group of mice was injected with WT SAS cells and the other group of mice was injected with FTO-deficient SAS cells using sterile techniques. After implantation of cells, mice were put back into their home cages, and routinely monitored for any pain and inflammation/infection until surgical removal of tumors. All procedures were approved by the Animal Ethics Committee of Kumamoto University (Approval ID: A29-016).

Cell lines

HOC313, MDA-MB-231, SAS, HeLa, 293FT, and MKN45 cells were maintained in Dulbecco's modified Eagle's medium (DMEM; GIBCO) containing 4,500 mg/L D-glucose, 2 mM L-glutamine, and 110 mg/L sodium pyruvate, with 10% heat-inactivated fetal bovine serum (Corning), at 37°C and 5% CO₂.

METHOD DETAILS

Transfection of siRNAs

Specific siRNAs for targeting *FTO* and control siRNA were purchased from Invitrogen. Transfections were conducted using Lipofectamine RNAiMAX (Invitrogen) at a final concentration of 50 nM according to the manufacturer's instructions. Cells were collected for subsequent experiments at 72 h after transfection.

Cell growth assay

Cells were seeded in 96-well plates (1×10^3 cells/well) 24 h before transfection. Cell growth was measured by adding 10 μ l of Cell Counting Kit-8 reagent (Dojindo) to each well. After incubation for 1 h at 37°C, the optical density at 450 nm was measured using a micro plate reader (Wako), and normalized against the measurement made on the first day.

Construction of a Fucci-expressing cell line

Plasmid vectors encoding mKO (pFucci-G1 Orange Cloning vector) and mAG (pFucci-S/G2/M Green Cloning vector) were purchased from MBL Life Science. Open reading frames of mKO and mAG were amplified and inserted into the *Xba*I and *Sal*I restriction enzyme sites in the pTomo vector (Addgene). A 10 μ g sample of pTomo-mAG or pTomo-mKO was then co-transfected with 7.5 μ g of psPAX2 (Addgene) and 5 μ g of pMD2G (Addgene) into HEK293FT cells using Lipofectamine 2000 reagent (Invitrogen). The medium was replaced at 12 h after transfection, and cells were incubated for 48 h for virus production. The supernatant containing Fucci-expressing lentiviruses was collected, and cell debris was removed with a 0.22 μ m filter unit (Millipore). A 1 mL sample of the virus stock was immediately used for infection of HOC313 cells cultured in a 6-well plate. At 4 days after infection, cells were plated in a 10 cm dish at a density of 40 cells/dish. Single colonies exhibiting both mAG and mKO fluorescence were cloned using a cloning disk (Sigma) and cultured for subsequent applications.

Time-lapse imaging of the cell cycle

For analysis of the cell cycle in Fucci-expressing HOC313 cells, cells were incubated in a CO₂ incubator equipped with a LCV110 microscope (Olympus). Fluorescence was calculated from three biological replicates (three independent experiments on different days). Each biological replicate is the average of at least five cells. Images were captured every 2 h, and the mAG and mKO fluorescence intensities were quantitated with ImageJ software.

Sorting of Fucci-expressing cells

Cells were treated with 0.05% trypsin and resuspended in phosphate-buffered saline (PBS). Cells expressing mAG or mKO were sorted using an SH800 cell sorter (SONY). A 561 nm laser was used to measure mKO fluorescence, and a 488 nm laser was used for mAG fluorescence. Cells were sorted into 15 mL tubes and centrifuged at 1,000 \times g for 5 min. The resulting cell pellet was used for subsequent experiments.

Cell cycle analysis by double thymidine blocking

The cell cycle was synchronized by the double thymidine blocking method as described previously (Sato and Kaida, 2016). Briefly, HOC313 cells were plated at 30% confluency, and incubated in the presence of 2 mM thymidine for 24 h. Cells were washed with PBS for three times, and the medium was replaced with thymidine-free medium. Cells were allowed to grow in the absence of thymidine for 12 h, then treated with 2 mM thymidine again and incubated for another 24 h. After incubation, cells were considered synchronized at the G1/S boundary. For cell cycle release, cells were washed three times with PBS and cultured in thymidine-free medium. Cells were collected every 4 h for RNA and protein extraction.

Gene editing by CRISPR/Cas9

To edit the potential m⁶A site in *cyclin D1*, a guide RNA (gRNA) was designed using Guide Design Resources (<https://zlab.bio/guide-design-resources>). The targeting sequence of the gRNA was 5'-AGTAACGTCACACGGACTAC-3'. A gRNA targeting exon 3 of FTO (5'-GTCTAATATAAACACACCG-3') was used to generate FTO knockout cells. Oligo DNAs were purchased from Hokkaido System Science and cloned into the LentiCRISPR v2 vector (Addgene). Lentivirus containing the gRNA was generated as described above, and HOC313 cells were infected with the lentivirus and selected using 2 μ g/ml puromycin (Sigma) for 3 days. Puromycin-resistant clones were further selected by the limited dilution method. After expansion of each clone, DNA was extracted using a DNeasy Blood & Tissue Kit (QIAGEN), and 2 μ l of genomic DNA was used for PCR amplification with Taq polymerase (TaKaRa). PCR products were separated on a 1% agarose gel, and corresponding bands were purified using a Gel Extraction Kit (QIAGEN). PCR fragments were further cloned into the pCRII-TOPO vector and subjected to DNA sequencing using a 3130 genetic analyzer (Applied Biosystems).

Immunocytochemistry and confocal imaging

Cells were fixed with 4% paraformaldehyde for 20 min and treated with 0.1% triton-PBS for 15 min. Samples were incubated with blocking solution (3% bovine serum albumin in PBS) for 1 h at room temperature, followed by incubation with anti-FTO antibody or anti-Myc antibody diluted in blocking solution at 4°C overnight. Cells were washed with PBS and incubated with secondary antibody conjugated with Cy5 for 1 h at room temperature. Cell nuclei were stained with 0.1 μ g/ml 4,6-diamidino-2-phenylindole (DAPI) for 10 min at room temperature. Cells were then analyzed using an FV3000 confocal microscope (Olympus). Fluorescence from mAG, mKO, and DAPI was examined by Fluoview software (Olympus).

RNA stability assay

HOC313 cells were treated with control siRNA or FTO-siRNA for 72 h. Cells were treated with actinomycin D at a final concentration of 1 μ g/ml. Cells were collected at 0, 2, 4, 8, and 12 h after addition of actinomycin D. Total RNA was extracted using TRIzol

(Thermo Fisher Scientific) followed by isopropanol precipitation. The expression level of *cyclin D1* was examined by quantitative PCR (qPCR).

Quantitative PCR

Total RNA (100 ng) was subjected to reverse transcription using Prime Script RT Master Mix (TaKaRa) according to the manufacturer's instructions. Reverse transcription was performed at 37°C for 15 min followed by enzyme inactivation at 95°C for 5 min using a Bio-Rad iCycler iQ PCR machine. cDNA was mixed using a TB GREEN Premix Ex-Taq2 kit (TaKaRa), and quantitative PCR was performed using Rotor Gene Q (QIAGEN). Primer sets were purchased from Hokkaido System Science and used at a final concentration of 0.2 μM. All qPCR assays were performed using at least three independent experiments with three different samples. Target gene expression levels were normalized against that of the 18S rRNA gene, and relative expression was calculated using the $2^{-\Delta\Delta Ct}$ method. Primer sequences can be found in [Table S1](#).

Protein extraction and western blotting

Protein from each cell line was extracted using lysis buffer (150 mM NaCl, 50 mM TRIS-HCl pH 8.0, 1% NP-40) with protease inhibitor cocktail (Roche). Cell lysates were sonicated and centrifuged at 10,000 × g for 5 min at 4°C. Protein concentrations were measured using a Pierce BCA protein assay kit (Thermo Scientific). Protein samples were separated by 10% sodium dodecyl sulfate-polyacrylamide gel electrophoresis (SDS-PAGE) and transferred onto a polyvinylidene fluoride (PVDF) membrane (Bio-Rad). Detection was performed using an ECLPlus chemiluminescence kit (GE Healthcare). All primary antibodies were used at a 1:1,000 dilution in 5% skim milk, and secondary antibodies were used at a 1:5,000 dilution in 5% skim milk. Actin was used as a loading control.

Dot blot analysis

Total RNA was isolated from HOC313 cells using TRIzol reagent, and 100 μg of total RNA was used for mRNA purification with an Oligotex-dT30 Super mRNA purification kit. Equal amounts of mRNA were spotted onto a Hybond N+ nylon membrane (GE Healthcare), followed by UV crosslinking at 254 nm and 100 μJ/cm². After blocking in 1% Block Ace (DS Pharma Biomedical) for 1 h, the membrane was incubated with anti-m⁶A antibody (Synaptic Systems) at a 1:1,000 dilution at 4°C overnight. On the following day, the membrane was washed five times with PBS containing 0.1% Tween-20. The membrane was then incubated with horseradish peroxidase (HRP)-conjugated anti-rabbit IgG (Invitrogen) at a 1:1,000 dilution in PBS for 1 h at room temperature. Chemiluminescence was detected using an ECL Plus kit (GE Healthcare).

LC-MS/MS

Total RNA was isolated from HOC313 cells using TRIzol reagent, and 100 μg was used for mRNA purification with an Oligotex-dT30 Super mRNA purification kit. A 50 ng sample of mRNA was digested with 2.5 U of Nuclease P1 (WAKO) and 0.2 U of bacterial alkaline phosphatase (TaKaRa) in 5 mM ammonium acetate and 20 mM HEPES-KOH (pH 7.0) for 3 h at 37°C. A 2 μl sample of digested mRNA was then subjected to ultra-high-pressure liquid chromatography coupled with triple quadrupole mass spectrometry using an LCMS8050 instrument (Shimadzu). Unmodified adenosine (A) and m⁶A were detected by the multiple reaction monitoring (MRM) method in positive ion mode. MRM parameters for A and m⁶A were as follows: A, precursor ion = m/z 268, product ion = m/z 136; m⁶A, precursor ion = m/z 282.3, product ion = m/z 150.

RNA-seq

Total RNA was isolated from *FTO* knockdown HOC313 cells using TRIzol reagent (cat. no. 15596-018; Thermo Fisher Scientific). A 2 μg sample of total RNA was subjected to mRNA purification using an Oligotex-dT30 Super mRNA purification kit (TaKaRa). Purified mRNA was fragmented into ~150 nt pieces by incubating with fragmentation buffer provided with the NEB Fragmentation Kit (NEB) at 94°C for 5 min. Fragmented mRNA was concentrated by ethanol precipitation, and half was submitted for RNA-seq (Novogene) and the other half was used for m⁶A immunoprecipitation followed by RNA-seq (MeRIP-seq). The library was prepared and sequenced using the HiSeq 2500 platform by Novogene.

MeRIP-seq

Immunoprecipitation of m⁶A-containing mRNA fragments was performed according to the protocol described above with modifications ([Fustin et al., 2013](#)). A 50 μL sample of protein G Dynabeads (cat. no. 10003D; Invitrogen) was washed three times with immunoprecipitation (IP) buffer (150 mM NaCl, 50 mM TRIS-HCl pH 8.0, 1% NP-40), resuspended in 500 μL of IP buffer, and mixed with 5 μg of m⁶A antibody (cat. no. 202003 Synaptic Systems) or 5 μg of control IgG antibody (cat. no. 2729S; Cell Signaling Technology). Antibodies were conjugated to protein G beads by gentle rotating for 1 h at 4°C, and beads were washed three times with IP buffer and resuspended in 500 μL of IP buffer. Fragmented mRNA was added and incubated for 3 h at 4°C in the presence of 40 U of RNasin (Promega). Following immunoprecipitation, beads were washed three times with IP buffer and resuspended in 250 μL of dilution buffer (10 mM TRIS-HCl pH 7.5). The mRNA fragments were recovered by addition of TRIzol, followed by chloroform extraction. Eluted RNAs were precipitated with ethanol and glycogen (TaKaRa), and dissolved in ultra-pure RNA-free water. The library was prepared and sequenced using the HiSeq 2500 platform by Novogene.

MeRIP-qPCR

A 25 μ L sample of protein G Dynabeads was washed with IP buffer three times and resuspended in 300 μ L of IP buffer, and 2 μ g of m⁶A antibody (cat. no. 202003; Synaptic Systems) or 2 μ g of control IgG antibody (cat. no. 2729S; Cell Signaling Technology) was added and mixed gently on a rotating wheel for 1 h at 4°C. Beads were then washed three times with IP buffer and resuspended in 300 μ L of IP buffer. Total RNA was purified from HOC313 cells using TRIzol reagent, and 500 ng of total RNA (Thermo Fisher Scientific) was added to the beads and mixed on a rotating wheel at 4°C for 3 h. Immunoprecipitated samples were washed with IP buffer three times and resuspended in 250 μ L of dilution buffer (10 mM TRIS-HCl pH 7.5). RNAs were recovered by addition of TRIzol, followed by chloroform extraction. Eluted RNAs were precipitated with ethanol and glycogen (TaKaRa) and dissolved in ultra-pure RNA-free water. Immunoprecipitated RNA was subjected to reverse transcription using Prime Script RT Master Mix (TaKaRa). Quantitative PCR was performed using TB GREEN Premix Ex-Taq2 (TaKaRa) on a Rotor Gene Q instrument (QIAGEN).

Purification of FTO protein

cDNAs of WT FTO, T4A FTO, T6A FTO, and T150A FTO were cloned into the pGEX4T1 vector (GE Healthcare), followed by transformation into *E. coli* strain BL21 (DE3). Expression of recombinant proteins was induced by addition of isopropyl β -D-1-thiogalactopyranoside (IPTG). Bacterial pellets were resuspended in ice-cold lysis buffer (50 mM TRIS-HCl pH 8.0, 300 mM NaCl, 1 mM EDTA pH 8.0, 1 mM EGTA, lysozyme, DTT, NP-40), followed by ultrasonication and centrifugation. GST-tagged proteins were bound to Glutathione Sepharose-4B beads (GE Healthcare) and eluted by addition of elution buffer (50 mM TRIS-HCl pH 8.0, 20 mM reduced glutathione). GST-tagged FTO recombinant proteins were stored at -80°C until needed for kinase assays.

Kinase assay

GST-FTO recombinant proteins were phosphorylated by recombinant Casein Kinase II (CKII, NEB) with 100 μ M ATP- γ -S (Sigma), 1X PK buffer (NEB) and p-Nitrobenzyl mesylate Alkylation reagent (Abcam) at 30°C for 1 h. Instead of CKII, BSA was added to the reaction mixture as negative control. The reaction was stopped by adding sample buffer, followed by heating at 90°C for 5 min. Samples were subject to SDS-PAGE and western blotting, and phosphorylation was detected by using anti-thiophosphate-ester antibody (Abcam).

Construction of siRNA- and CRISPR-insensitive human FTO

To generate siRNA-insensitive FTO cDNA, the targeting sequence of siRNA in human *FTO* (5'-AGCAGTGTATCTGAGGAGCTCCA TAA-3') cDNA was mutated to 5'-AGtAGcGTcTcCGAaGAaCTaCAcAA-3' by site-directed mutagenesis to preserve the coding amino acids. HeLa cells were co-transfected with siRNA against endogenous *FTO* mRNA and plasmids carrying mutant *FTO* using Lipofectamine 2000 (Invitrogen). To generate CRISPR-insensitive *FTO*, the targeting sequence of gRNA in human *FTO* cDNA (5'-GTCTAATATAAAACACCG-3') was mutated to 5'-GTCTAATATAAAgCATaCtG-3'. FTO knockout SAS cells were transfected with the constructs using Lipofectamine 3000 (Invitrogen).

Immunoprecipitation of the FTO-RNA complex

HeLa cells were transfected with plasmid encoding *Myc-FTO* for 48 h and irradiated (4000 \times $\mu\text{J}/\text{cm}^2$) at 254 nm using a UV crosslinker (Funakoshi). Cells were resuspended in subcellular fractionation buffer (250 mM sucrose, 20 mM HEPES pH 7.4, 10 mM KCl, 1.5 mM MgCl_2 , 1 mM EDTA, 1 mM DTT, protease inhibitor cocktail). Cell lysates were passed through a 27-G needle 10 times using a 1 mL syringe. After incubation on ice, cell lysates were centrifuged at 800 \times g for 5 min. The supernatant was centrifuged again at 6000 \times g, and the resulting supernatant was used as the cytosolic fraction. The pellet was resuspended in fractionation buffer and passed through the 27-G needle again. After a brief centrifugation at 800 \times g for 10 min, the pellet was resuspended in lysis buffer (150 mM NaCl, 50 mM TRIS-HCl pH 7.4, 0.1% NP40, 0.1% SDS, protease inhibitor cocktail), followed by a brief sonication. The nuclear lysate was centrifuged at 10,000 \times g for 10 min to remove the DNA pellet, and the resulting supernatant was used as the nuclear fraction. Cytosolic and nuclear lysates were immunoprecipitated with anti-Myc antibody and normal mouse IgG as negative control. The anti-Myc antibody used for immunoprecipitation was also used in immunostaining experiment as described above.

Xenograft model

To generate the subcutaneous xenograft model, 7-week-old male BALB/c-nu (CAnN.Cg-Foxn1^{nu}/CrIcrI) mice were used. SAS WT cells or SAS *FTO* knockout cells were suspended in PBS/Matrigel Matrix (1:1) at a density of 3×10^6 cells/100 μ L. Cell suspensions were injected into mice subcutaneously, and allowed to grow *in vivo*. Mice were sacrificed by acute cervical dislocation, and tumors were removed by dissection.

Data analysis

RNA-seq data from three independent experiments were uploaded to the main Galaxy Server and analyzed using Galaxy tools unless specified otherwise. Data quality control was performed using FASTQC, followed by trimming with the Trimmomatic tool. Alignment against the human genome (GRCh37/hg19) was performed using HISAT2. The HTSeq-count tool was used to calculate the number of reads mapped to known genes, and differential gene expression was determined using DESeq2. Genes were considered significantly altered if the absolute fold-change was > 2 and the Benjamini-Hochberg *p*-value was < 0.05 . Pathway analysis was performed using the Enrichr web server.

For analysis of MeRIP-seq data, quality control was performed using FASTQC, followed by trimming using Galaxy tools. Alignment against the human genome (GRCh37/hg19) was performed using HISAT2. RNA-seq data (as input) and MeRIP-seq data (as m⁶A samples) were analyzed using MACS2 and exomePeak tools for peak calling, and exomePeak data were submitted to the Guitar package to examine the distribution of m⁶A peaks across transcript lengths. The HTSeq-count tool was used to calculate the number of reads mapped to known genes, and genes overlapping in two independent MeRIP-seq mRNA datasets from HOC313 cells were considered m⁶A-containing genes. For all BAM files generated from m⁶A-IP samples, control IgG-IP samples, and input samples, the bamCoverage tool was used to generate bigWig files of read coverage with reads per kilobase of transcript per million mapped reads (RPKM) normalization. For examination of m⁶A density, the read coverage of *cyclin D1* in m⁶A samples was first normalized against the corresponding IgG samples, followed by normalization against input samples.

For analysis of MeRIP-qPCR results, the Ct value of *cyclin D1* in m⁶A-IP samples was first normalized against control IgG-IP samples to subtract the background. The value was then normalized against the Ct value of input samples to calculate the proportion of m⁶A modification.

QUANTIFICATION AND STATISTICAL ANALYSIS

All data were analyzed using GraphPad Prism 8 software. Unpaired Student's t tests or Mann Whitney tests were used to assess differences between two groups, and two-way ANOVA tests followed by Tukey's multiple comparisons were used to examine differences among multiple groups. A two-tailed *p-value* of 0.05 was considered significant. Data are presented as means ± SEM.

DATA AND CODE AVAILABILITY

RNA sequencing data from this work are available under accession number GSE133857. This dataset is associated with [Figure 2](#).

Cell Reports, Volume 31

Supplemental Information

FTO Demethylates *Cyclin D1* mRNA and Controls Cell-Cycle Progression

Mayumi Hirayama, Fan-Yan Wei, Takeshi Chujo, Shinya Oki, Maya Yakita, Daiki Kobayashi, Norie Araki, Nozomu Takahashi, Ryoji Yoshida, Hideki Nakayama, and Kazuhito Tomizawa

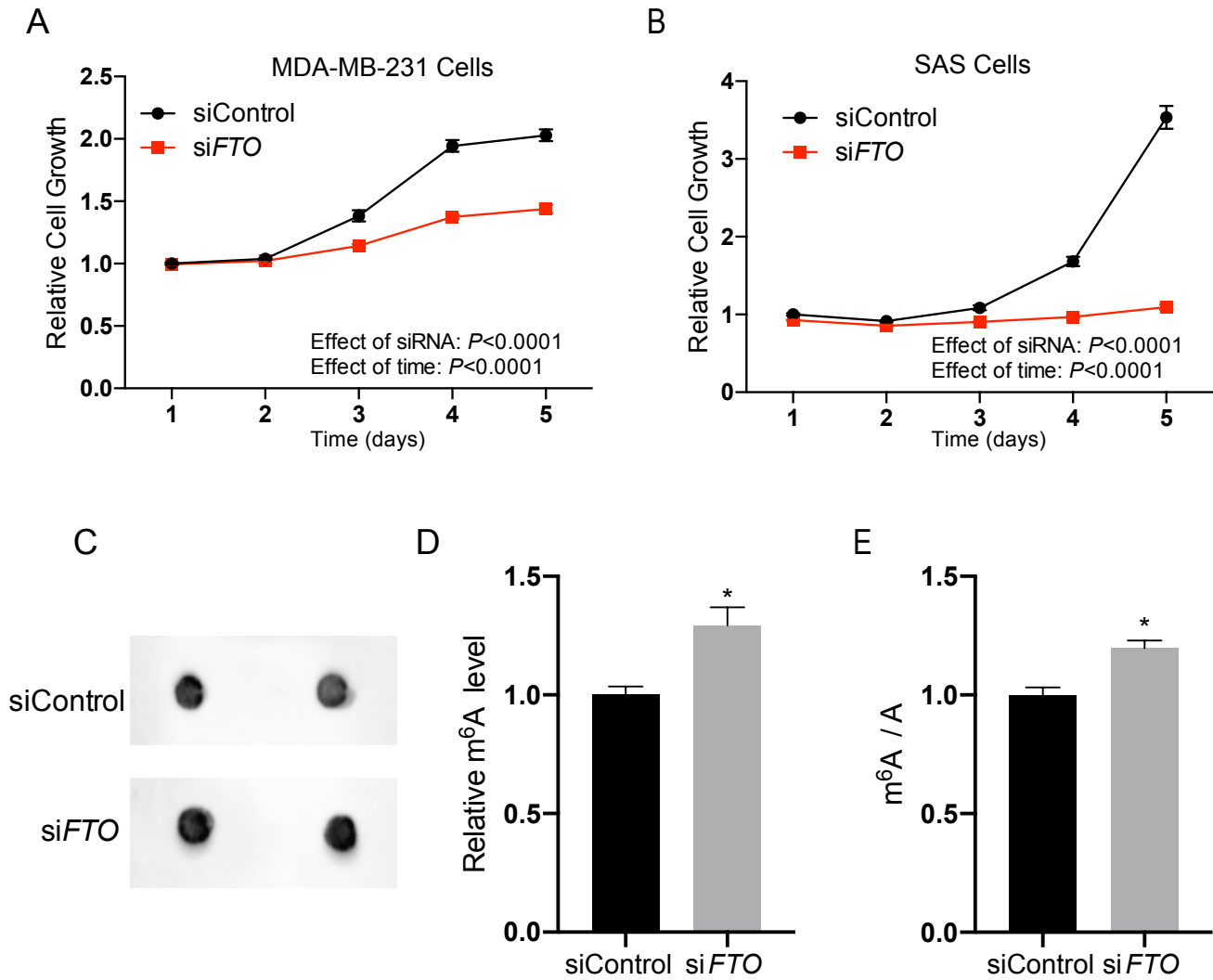


Figure S1. *FTO* knockdown increases m⁶A modification and suppresses cell growth (Related to Figure 1).

(A, B) Growth rate of MDA-MB-231 and SAS cells. Two-way ANOVA was used to calculate significant differences between groups and timepoints. (C) Dot blot analysis of m⁶A modification of total RNA isolated from HOC313 cells treated with control siRNA (siControl) or *FTO*-siRNA (siFTO). (D) Quantitation of the intensities of m⁶A dots (n = 4 for each group; * $p < 0.05$ by Student's t-test). (E) LC-MS/MS analysis of m⁶A modification of mRNA isolated from HOC313 cells treated with siControl or siFTO (n = 3 for each group; * $p < 0.05$ by Student's t-test). The abundance of m⁶A was normalized against the abundance of adenosine (A) (n = 3 for each group; * $p < 0.05$ by Student's t-test).

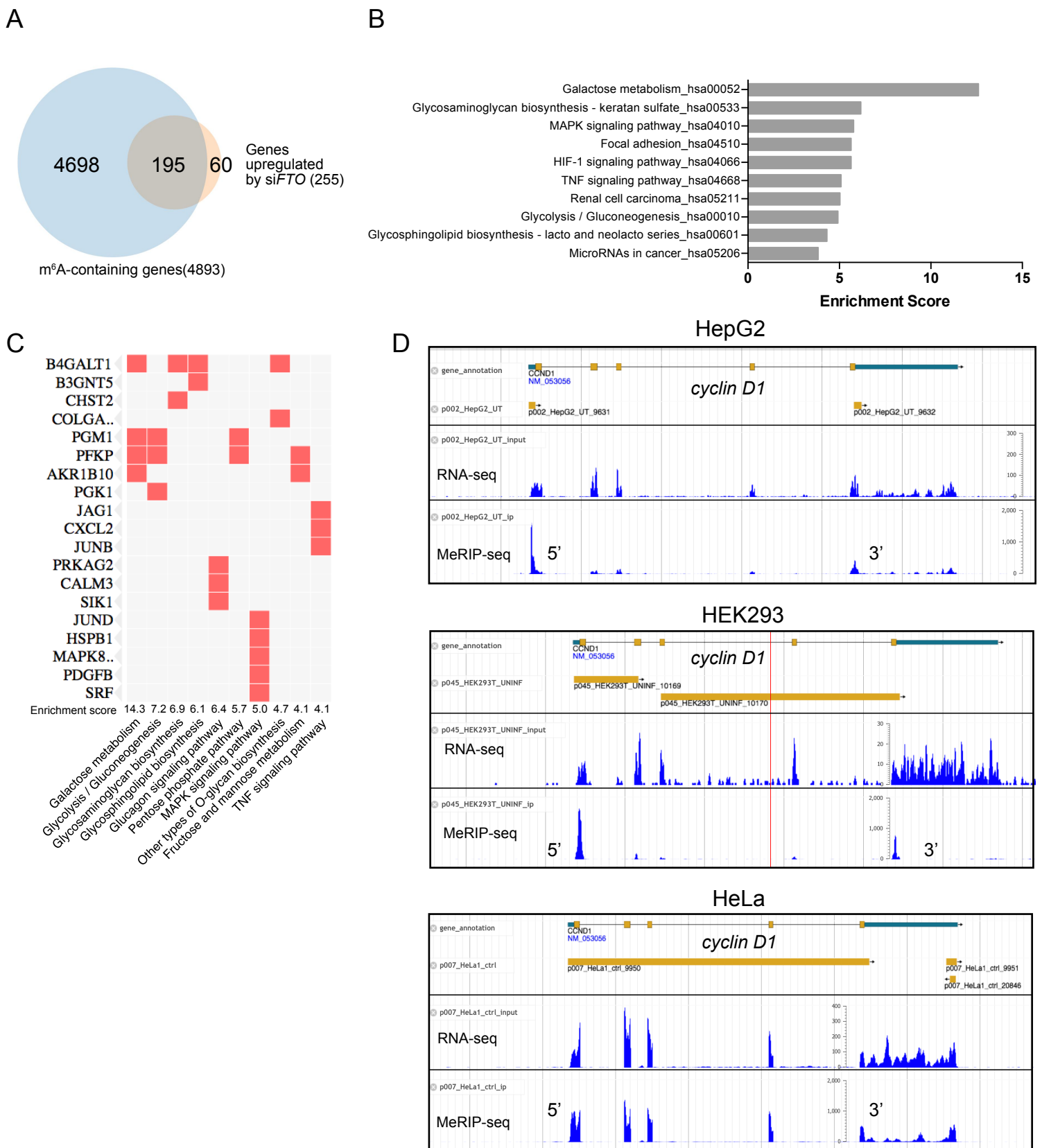


Figure S2. Transcriptome analysis of m⁶A-containing genes upregulated in *FTO* knockdown cells (Related to Figure 2).

(A) Venn diagram showing 195 genes overlapping between genes containing the m⁶A modification and genes upregulated in *FTO* knockdown cells. (B) Pathway analysis of genes upregulated in *FTO* knockdown cells. (C) Pathway analysis of m⁶A-containing genes upregulated in *FTO* knockdown cells. (D) RNA-seq and MeRIP-seq results from HepG2, HEK293, and HeLa cells retrieved from MeT-DB V2.0. For each cell line, the upper panel shows the gene structure of *cyclin D1*, the middle panel shows the RNA-seq read coverage of *cyclin D1*, and the lower panel shows the MeRIP-seq read coverage of m⁶A in *cyclin D1*. Note that the scale of coverage is different between the middle and lower panels.

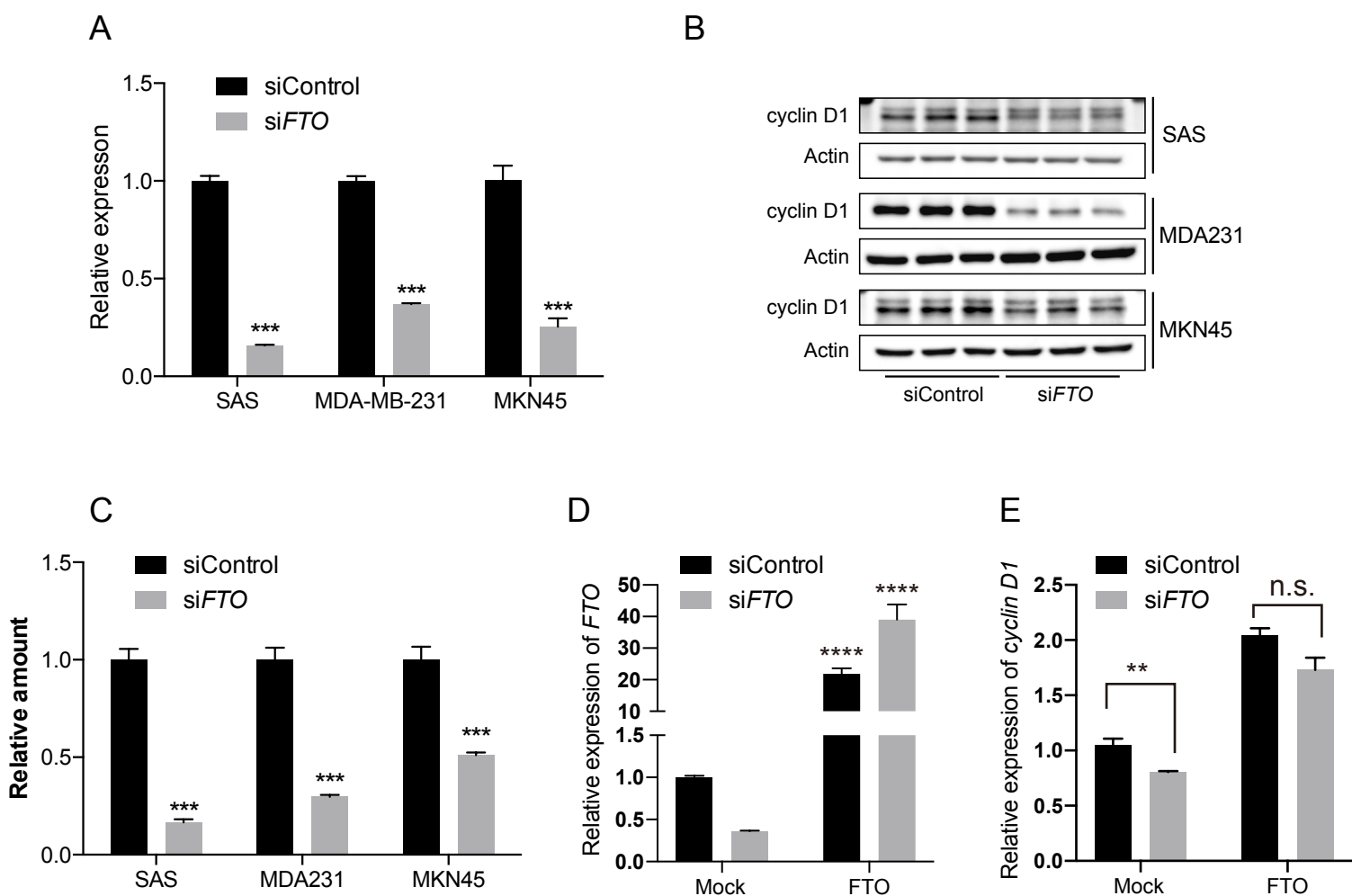


Figure S3. Suppression of *cyclin D1* at mRNA and protein levels in multiple cell lines upon *FTO* knockdown (Related to Figure 3).

(A) Relative expression levels of *cyclin D1* in SAS, MDA-MB-231, and MKN45 cells treated with control siRNA (siControl) or *FTO*-siRNA (siFTO; n = 3 for each group; ****p* < 0.001 by Student's t-test). SAS: siControl: 1.0±0.03 vs. siFTO: 0.16±0.004, MDA-MD-231: siControl: 1.0±0.02 vs. siFTO: 0.34±0.005, siControl: 1.0±0.07 vs. siFTO: 0.26±0.04. (B) Western blotting analysis showing a decrease in cyclin D1 protein in SAS, MDA-MB-231, and MKN45 cells treated with siControl or siFTO. (C) Quantitation of cyclin D1 protein levels (n = 3 for each group; ****p* < 0.001 by Student's t-test). SAS: siControl: 1.0±0.06 vs. siFTO: 0.17±0.02, MDA-MD-231: siControl: 1.0±0.06 vs. siFTO: 0.30±0.009, siControl: 1.0±0.07 vs. siFTO: 0.51±0.01. (D and E) HeLa cells were transfected with siControl or siFTO followed by transfection of mock plasmid or human *FTO* plasmid carrying synonymous mutations in nucleotides corresponding to siRNA-targeting sites. Expression levels of *FTO* (D) and *cyclin D1* (E) in each group are shown (n = 3-4 for each group; *****p* < 0.001 versus cells transfected with control siRNA and mock plasmid by Student's t-test adjusted for multiple comparison; n.s. = not significant). (D) *FTO* levels: siControl + Mock: 1.0±0.02, siFTO + Mock: 0.36±0.008, siControl + *FTO*: 21.8±1.75, siFTO + *FTO*: 39.0±4.78. (E) *cyclin D1* levels: siControl + Mock: 1.0±0.06, siFTO + Mock: 0.81±0.009, siControl + *FTO*: 2.0±0.07, siFTO + *FTO*: 1.7±0.11.

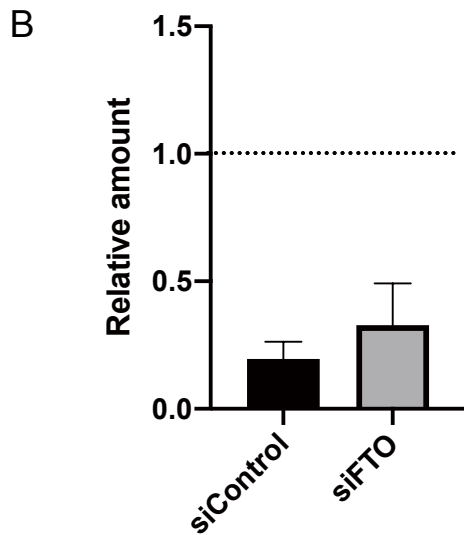
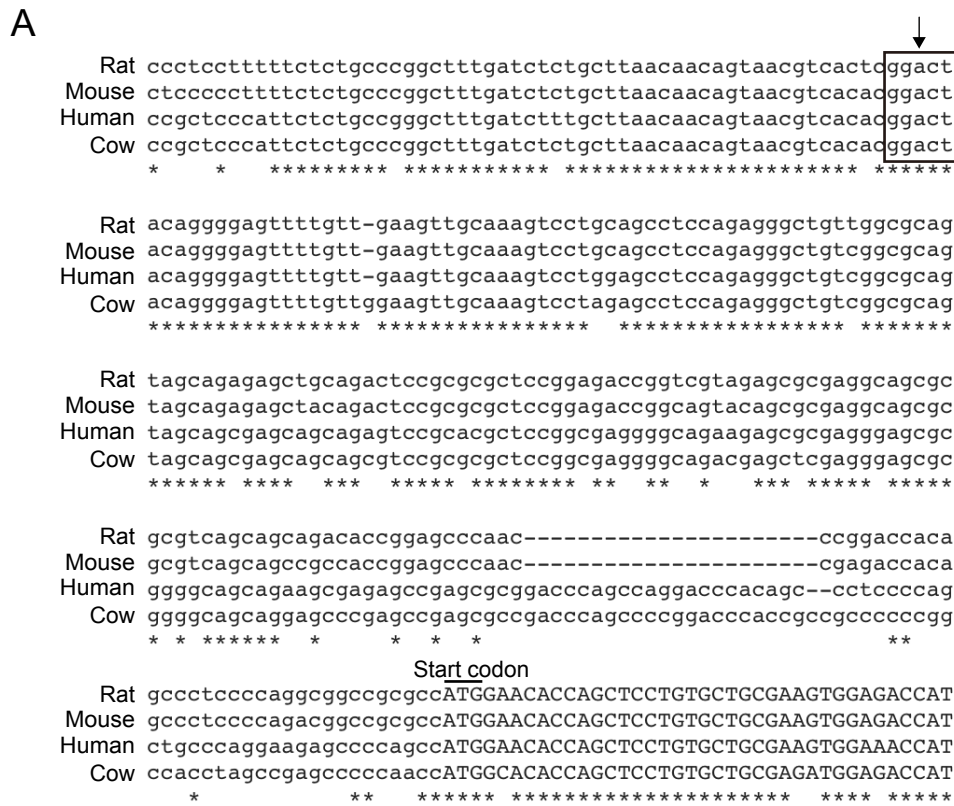


Figure S4. Alignment of *cyclin D1* genes across species (Related to Figure 4).

(A) Alignment of the 5' -UTR of rat, mouse, human, and cow *cyclin D1* genes. The box indicates the conserved m⁶A motif. The arrow indicates the potential m⁶A site. The translation start site is labeled as the start codon. (B) HOC313 cells carrying *Mut-cyclin D1* were transfected with control siRNA (siControl) or *FTO*-siRNA (siFTO). m⁶A modification of *cyclin D1* was examined by MeRIP-qPCR (n = 3 for each group), and normalized to m⁶A modification level in WT HOC313 cells. siControl: 0.20±0.07, siFTO: 0.33±0.16, WT HOC cells: 1.0±0.13.

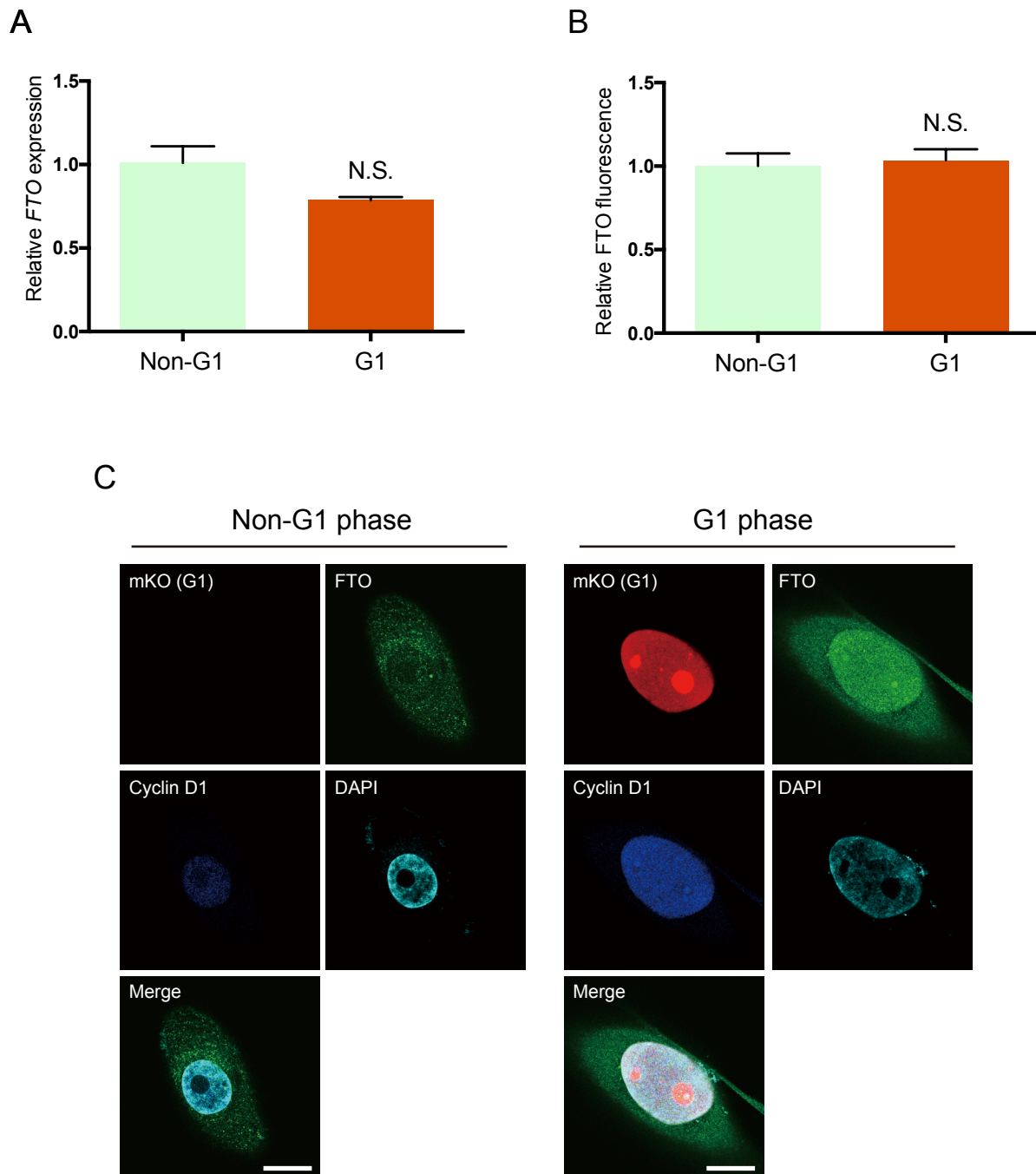


Figure S5. *FTO* expression levels in non-G1 and G1 cells (Related to Figure 6).

(A) Sorting of Fucci-expressing HOC313 cells into mKO-expressing G1 phase cells and mAG-expressing non-G1 phase cells. *FTO* mRNA levels are not different between G1 and non-G1 cells. (B) Staining of Fucci-expressing HOC313 cells with anti-*FTO* antibody. The intensity of *FTO* fluorescence is not different between G1 and non-G1 cells. (C) HOC313 cells expressing mKO were stained with DAPI, anti-*FTO* antibody, and anti-cyclin D1 antibody. Bar = 20 μ m.

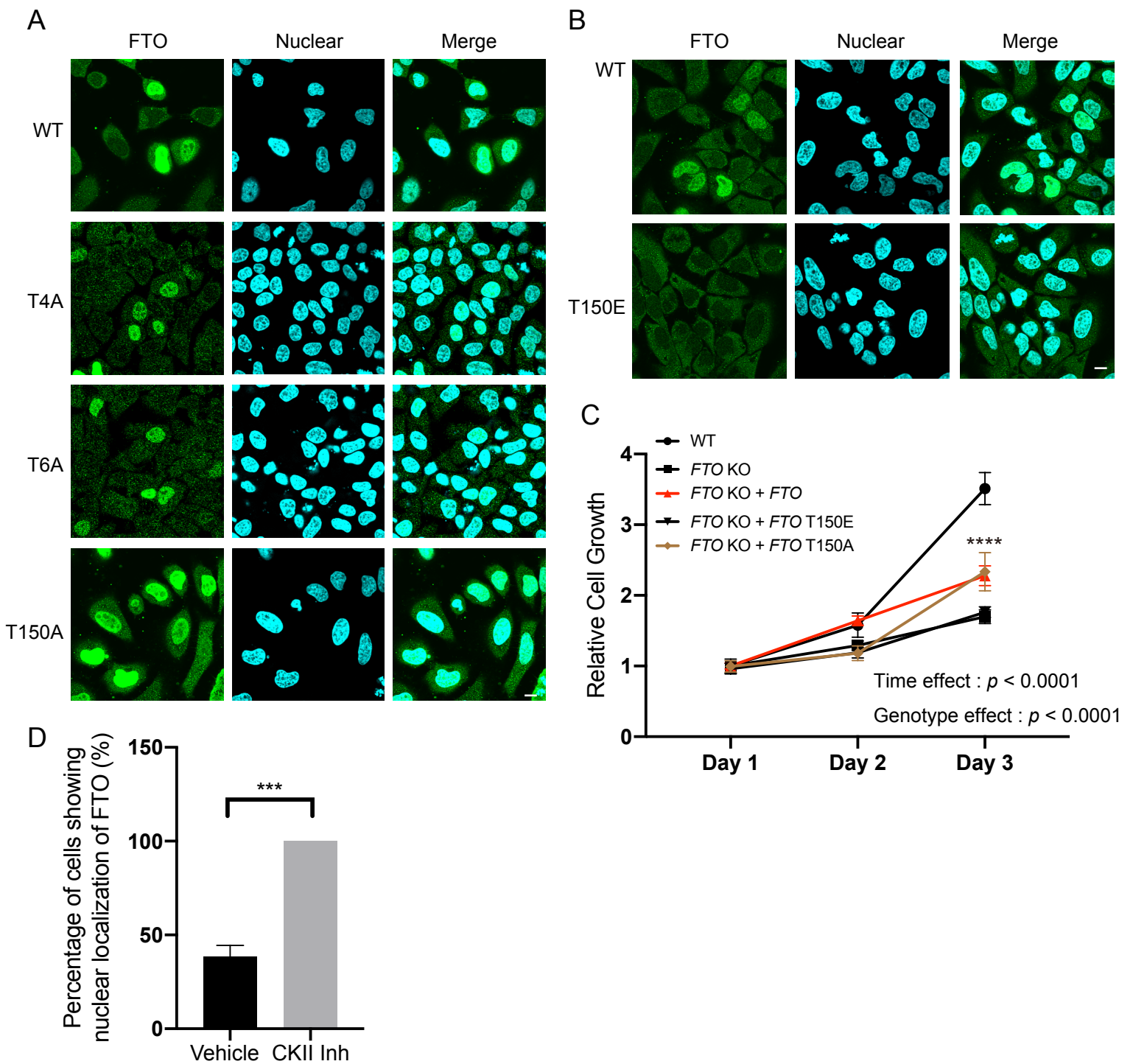


Figure S6. Phosphorylation regulates nucleocytoplasmic shuttling of FTO (Related to Figure 7).

(A) *FTO* WT, *FTO* T4A, *FTO* T6A, and *FTO* T150A were conjugated to a Myc-tag at the C-terminus, and transfected into HeLa cells. HeLa cells were immunostained with anti-Myc antibody to visualize exogenous FTO. Representative images of HeLa cells expressing each type of *FTO* are shown. Bar = 10 μ m. (B) *FTO* WT and *FTO* T150E were transfected into HeLa cells, and representative images of HeLa cells are shown. Bar = 10 μ m. (C) Relative cell growth measured using WST-8 assays in WT SAS cells, *FTO* knockout (KO) SAS cells, and *FTO* knockout SAS cells transiently expressing human *FTO*, *FTO* T150E, and *FTO* T150A (n = 4 for each group). Two-way ANOVA followed by multiple comparison tests were performed to calculate the statistical significance between groups at each timepoint. Day 3 = *FTO* KO + *FTO* versus *FTO* KO, **** p < 0.0001; *FTO* KO + *FTO* T150E versus *FTO* KO, not significant; *FTO* KO + *FTO* T150A versus *FTO* KO, **** p < 0.0001. (D) HOC313 cells were stained with anti-FTO antibody and DAPI. The percentage of cells displaying nuclear localization of FTO is shown (n = 3 biological replicates for each group; **** p < 0.001 by Student's t-test).